Diploma Thesis

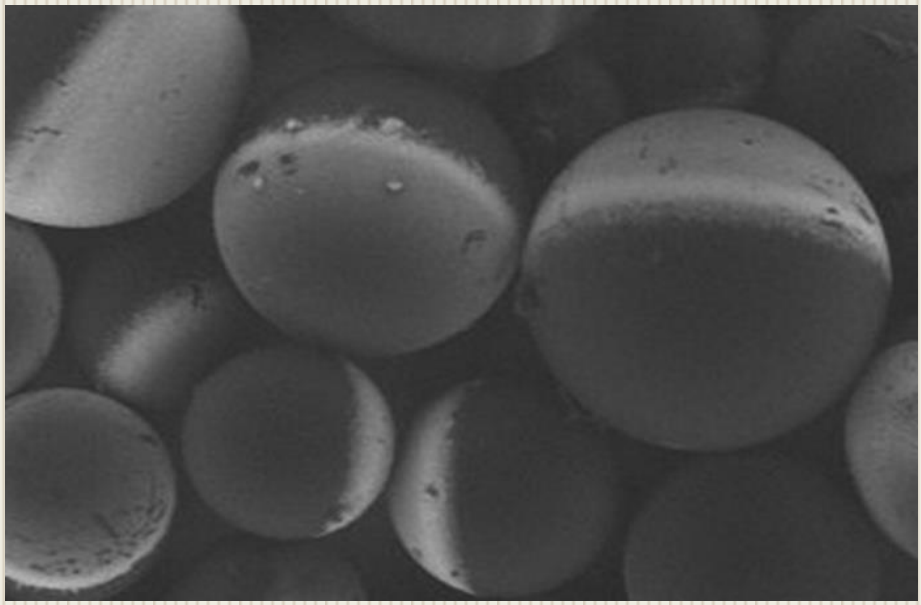

pH-responsive hybrid Janus nanoparticles

Kokolakis Nikolaos-Dimitrios

Supervisor : Associate Professor Maria Vamvakaki

University of Crete
Department of Materials Science and Technology
Foundation for Research & Technology - Hellas
Institute of Electronic Structure and Laser

Heraklion , March 2015

Table of Contents

Acknowledgements

I would like to express my special thanks to my supervisor Dr Maria Vamvakaki, for giving me the opportunity to work in this project.

A special thanks to Panagiotis Falireas for the synthesis of Janus nanoparticles, supervising and for his precious help to complete my study.

Finally, I would like to express my thanks to all my colleagues Maria Kaliva, Fanis Krasanakis, Andreas Pamvouxoglou, Lefteris Koufakis and Xara Flouraki for helping me in everything that I needed.

Abstract

Janus particles are named after the two-faced ancient Roman god Janus, based on the chemical and physical anisotropy that these particles exhibit. Soft Janus particles represent a fascinating group of polymeric materials, which open new ways in academia and industry.

In this study we present the characterization of silica nanoparticles with asymmetric grafting of polymer chains from their surface. Hybrid Janus nanoparticles consist of an inorganic silica core and grafted polymer chains. The multistep reaction commenced with the stabilization of a styrene/methanol Pickering emulsion using amine-functionalized silica nanoparticles (D = 100 nm) as stabilizers. The solvent exposed surface of the silica nanoparticles was modified with an atom transfer radical polymerization (ATRP) initiator. After the functionalization, polystyrene was dissolved yielding Janus nanoparticles bearing ATRP initiating sites. Next, surface-initiated ATRP of t-BuA was carried out from the initiator-functionalized hemisphere of the silica nanoparticles followed by the removal of the bromide end groups to obtain halogen free P(t-BuA) polymer chains. Subsequently, functionalization of the second hemisphere with the ATRP initiator was performed. Acid hydrolysis of P(t-BuA) led to oppositely charged Janus particles decorated with PAA polymer chains on the one hemisphere and an amine-functionalized hemisphere.

The amount of grafted polymer chains from the surface of the particles was determined by Thermogravimetric Analysis (TGA), while the molecular weights and molecular weight distributions of the polymers formed in solution were determined by Gel Permeation Chromatography (GPC). The morphology of the polymer-silica Janus particles was studied with Scanning Electron Microscopy (SEM).

The successful hydrolysis of the P(*t*-BuA) chains was investigated with Fourier Transform Infrared (FT-IR) Spectroscopy. The pH-responsive behaviour of the particles in an aqueous solution was studied using potentiometric titration and dynamic light scattering.

Abbreviations

APTES	(3-Aminopropyl) triethoxysilane
ATRP	atom transfer radical polymerization
DLS	dynamic light scattering
FT-IR	Fourier Transform Infrared Spectroscopy
GPC	gel permeation chromatography
PAA	poly(acrylic acid)
P(t-BuA)	poly(tert-butyl acrylate)
$\boldsymbol{R_H}$	hydrodynamic radius
SEM	scanning electron microscopy
TGA	thermogravimetric analysis
THF	tetrahydrofuran

CHAPTER 1. Introduction

1.1 Anisotropic particles with multicompartment and Janus architecture

Living organisms serve as a source of inspiration for the technological development of materials. Natural materials are characterized by hierarchical structures at scales ranging from nanometre to millimetres. The demand for advanced functions and novel properties has led to the most promising research area called nanotechnology that governs material science. In the last twenty years, nanotechnology is without any doubt one of the most important technologies of the 21st century. Scientific research has led to a much more sophisticated set of tools to control the size, shape, dispersity and surface chemistry of nanoparticles. Hence, the complexity of possible structures offers completely new ways to use particles for specific applications.

One of the most promising research topics is the design of materials that desired constitute the building blocks to create new structures by their spontaneous self-assembly. Today, the production of nanoparticles consisting of both an inorganic and an organic (polymeric) part employs a wide variety of techniques and such nanoparticles are proposed for applications in almost all industrial fields. However, most techniques create particles with isotropic surface properties, and for this reason new strategies to synthesize nanoparticles with asymmetric properties, constitute a challenge for scientific research.

The past few years we have seen an unbelievable revolution in materials science, especially in the preparation and design of nano- or micro-sized anisotropic particles such as patchy, multicompartment and Janus particles. These particles have attracted great attention since they can be used for the creation of new structures with new specific properties and can find unique applications due to their non-centrosymmetric features.

O Reilly *et al.* classified the key features of all types of anisotropic particles such as Janus particles, multi-compartment particles, patchy particles, patchy Janus particles and patchy multi-compartment particles in a number of excellent reviews, [1, 2] and compared their structural properties with respect to their preparation techniques. [3]

1.2 Janus Particles

In his Nobel lecture, in 1991, De Gennes highlighted the term “Janus Particles”, which is named after the double-faced Roman god. The Janus Particles are a particular type of nanoparticles whose surfaces have two or more distinct physical properties. [4] After their introduction, Janus particles turned out to be a very promising group of nanoparticles for a lot of scientists. Originally the term Janus particle was coined by C. Casagrande in 1988 to describe spherical glass particles with one of the hemispheres hydrophilic and the other hydrophobic. This feature of the Janus nanoparticles allows two different types of chemistry to occur on the same particle. The simplest case of a Janus nanoparticle is achieved by dividing the nanoparticle into two distinct parts, each of them is either made of a different material, or bear different functional groups. [5] For example, a Janus nanoparticle may have one-half of its surface composed of hydrophilic groups and the other half of hydrophobic groups. [6]

1.2.1 Classification

Janus particles turned out to be a very promising group of nanoparticles for a lot of scientists and lead to a new class of colloidal structures among the micro- or nano-sized particles. The terminology is based on the special architectural feature of having two sides or at least two surfaces with different chemistry or polarity. In general, Janus particles can be divided into three super ordinate classes according to their architecture and dimensionality (Figure 1.1). Most commonly, spherical (3D) Janus particles as depicted below, in addition, two types of cylinders (1D) and two types of disc-like particles (2D) are shown. [7, 8]

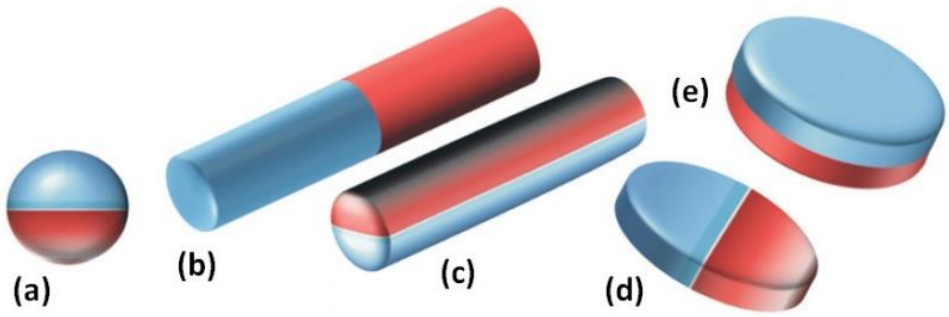

Figure 1.1: Overview of possible Janus particle architectures: (a) spherical, (b,c) cylindrical, (d,e) disc-shaped.

1.2.2 Properties and Applications

1.2.2.1 Properties

Janus particles and in particular their applications are the subject of research for many scientists. There are several examples which demonstrate the use of Janus particles in new structures with advanced properties. A few of these examples include their use as stabilizers in emulsions, catalysts in reactions, drug delivery systems, surfactants, as well as in biological, electronic and textile applications. The number of publications on Janus particles increased rapidly in the last few years with focus on the synthesis and applications of Janus particles. [8]

Due to this special non-centrosymmetric structure, the synthesis of Janus particles is very difficult. On the other side, the lack of centrosymmetry in Janus systems has led to the discovery of new properties as well as unusual aggregation behaviour into superstructures.

The ability of a material to self-assemble into complex hierarchical superstructures is encoded into its architecture. The understanding of self-assembly processes is of profound interest, for the fabrication of complex structures. Janus particles possess the unique feature of being non-centrosymmetric and thus many investigations have been concerned with the solution properties and self-assembly behaviour of these particles. [9-14] Janus particles with two distinct faces exhibit unique properties in solutions.

In an aqueous solution, amphiphilic Janus particles form two kind of aggregates. The first type of aggregates is small clusters whereas the second kind of aggregates is larger than the first and has been termed ‘super micelles’. On the other hand, Janus particles in aqueous solution with polymer chains of the same charge were well dispersed in the solvent, while these with polymers of opposite charge formed finite sized clusters due to the strong dipolar interactions between the Janus nanoparticles.

The experimental studies are complemented by a range of computer simulation approaches discussing self-assembled structures and phase diagrams of JPs of different architectures. Due to the difference in nature of their interactions, the self-assembly of dipolar Janus particles [13] and amphiphilic Janus particles [14] are completely different.

Predictions by computer simulations describe a rich phase diagram for simple bipolar Janus particles (in Figure 1.3) with a variety of self-assembled structures. Molecular dynamic simulations by Goyal *et. al*. identified FCC, HCP, and BCC lattices at high packing fractions and fluid, string-fluid, and gel phases at lower packing fractions. [15]

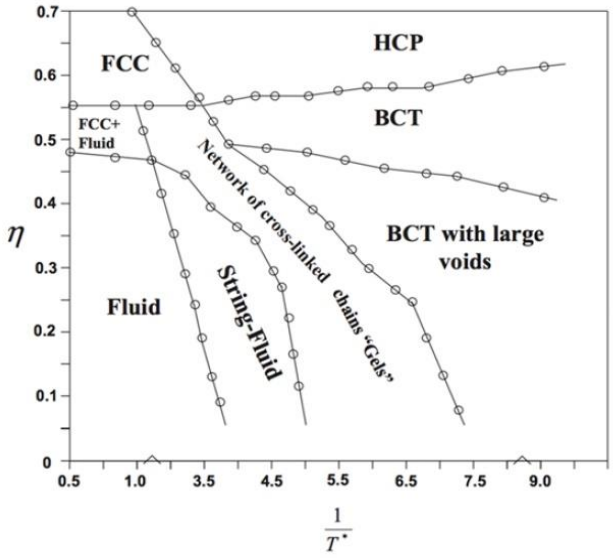

Figure 1.3: Self-assembly and phase behavior of dipolar Janus particles.

The self-assembly behaviour of solid beads, in which the hemispheres were amphiphilic, [14, 16] hydrophobic hemisphere on one face and charged on the other, was investigated both experimentally and by computer simulations. In water, the interactions can range from an extreme of hydrophobic attraction, when the hydrophobic sides face each other, to the limit of electrostatic repulsion when the two charged sides face one another. Although the interactions between these particles have an anisotropy that is similar to that of dipolar particles the resulting aggregates have structures that differ greatly from those of dipolar particles. The hydrophobic attraction and electrostatic repulsion are modulated further according to particle orientation due to their Janus character.

Similarly, to analyse the interactions between charged Janus particles it is useful to consider a polar axis pointing north–south through the hemispheres. For this case spheres which had a positive charge on one hemisphere and negative charge on other hemisphere was used. If we define that the Janus particles lie in the same plane (Figure 1.2A) the interaction changes smoothly from repulsive to attractive depending on how the particles face one another and it's illustrated in Figure 1.2B over a narrow range of rotation angle. In the general case where the polar axes passing through the hemispheres do not lie in the same plane (Figure 1.2C) the interaction potential depends on the relative orientation as well as on separation. This multidimensional parameter space illustrates the rapid increase of complexity as one goes beyond the classical concept of isotropic potentials.

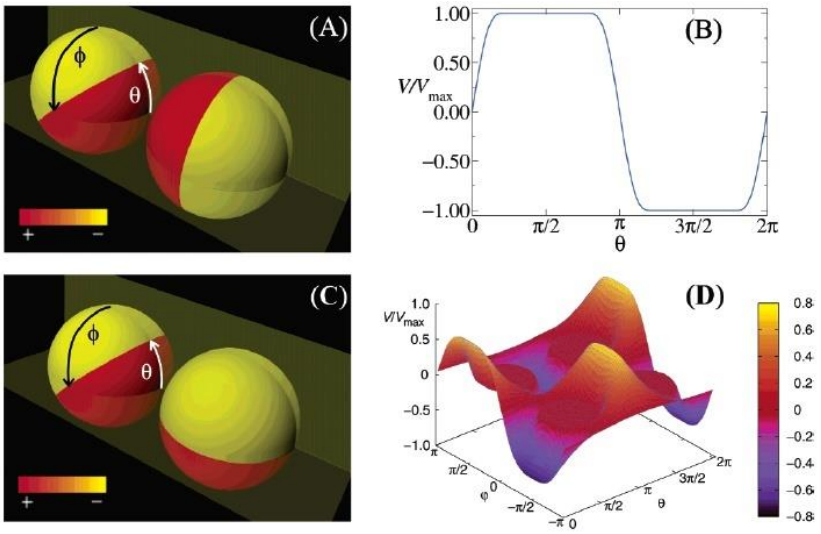

Figure 1.2: Interaction potential between two particles with bipolar charge. The right object is fixed; the angles (θ, φ) indicate the orientation of the left object.

In attractive systems, the number of charged particles in an aggregate is dependent on the size of the aggregates. It has been shown [13] that with increasing number of particles the size of the aggregates increases. In principle, there appears to be no limit to the size of clusters that can form from these electrostatic interactions. Each cluster of larger size is energetically more stable than all of the smaller ones and therefore the clusters might merge into larger ones, therefore a large concentration of clusters is needed. Due to the charge anisotropy of particles it is logical to conclude that energetically the positive side of one cluster will attract the negative side of another cluster, resulting in facile assembly into even larger aggregates.

The surface activities of nanoparticles with amphiphilic properties have been investigated by many research groups. The main characteristic of Janus nanoparticles is the capability of possessing both hydrophilic and hydrophobic parts. In daily life, Janus nanoparticles are used to stabilize emulsions and dispersions such as milk or cosmetics. [17]

1.2.2.2 Applications

One example that shows the numerous applications of Janus particles was shown by Nisisako *et al.* who made use of the electrical anisotropy of Janus particles, filled with white and black pigments in both hemispheres, in electronics. [18] These particles were used to make switchable screens by placing a thin layer of these spheres between two electrodes. Upon changing the applied electric field, the particle orientation is changed, their black sides goes to the anode and their white sides to the cathode. The orientation and the colour of the display can be changed by simply reversing the electric field. With this method, it may be possible to make very thin, robust and environmentally stable displays.

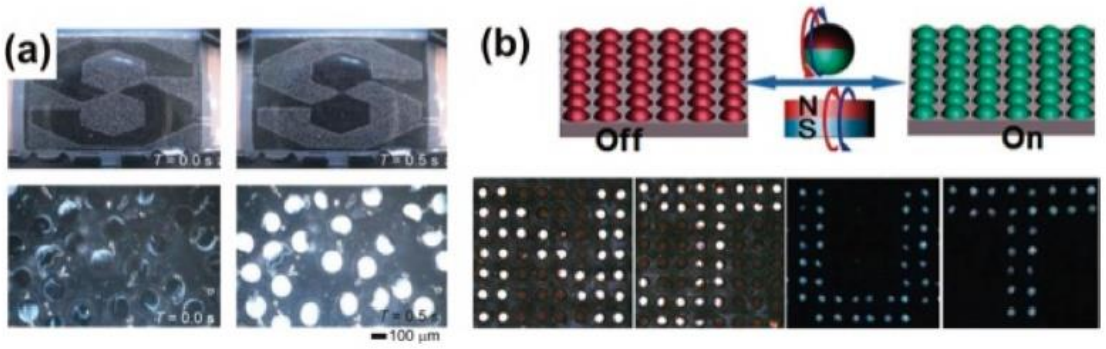

Figure 1.4: E-paper panel displays based on (a) AC-field-based switching of Janus microspheres with black and white sides and (b) magnetic actuation of JPs with one super-paramagnetic and one fluorescent side.

Janus particles can also be used as efficient and unique optical probes for biological interactions or rheological measurements in confined space. In recent years, this concept has been brought forward by Behrend and co-works, [19-21] who used Janus beads coated on one side with metal. Being placed into a specific environment, these particles blink on and off depending on the surrounding conditions.

Another interesting effect which potentially finds applications in nanoscience is the self-propulsion induced by catalytically active Janus beads with a spatially asymmetric distribution of the reaction site. [22, 23] These particles are used in nanomedicine, as they exhibit an increased diffusion coefficient. This makes drug-delivery vehicles more efficient because in less time it allows them to screen a larger volume for docking sites.

Ryan *et al.* used polystyrene particles coated on one side with a thin platinum layer and studied their diffusion in dependence of the concentration of hydrogen peroxide. Hydrogen peroxide was degraded by platinum into two reaction products (O_2(g) and H_2O). This induces a non-equilibrium distribution and local gradients of partly gaseous products propelling the particle forward due to osmotic pressure.

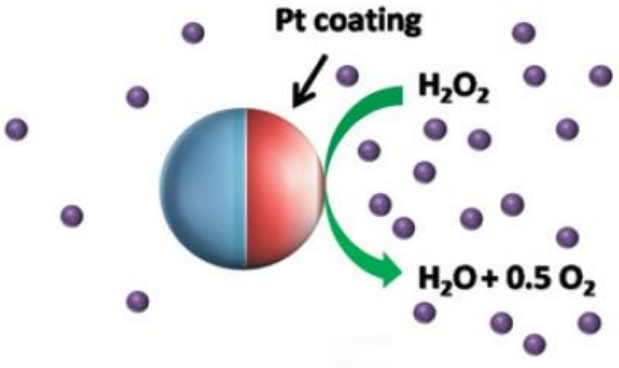

Figure 1.5: Self-propulsion of a Janus particle via the asymmetric distribution of reaction products.

1.3 Preparation Methods

In the past decade, the synthesis of Janus particles has achieved great progress due to the development of appropriate synthesis methods. The synthesis methods can be classified into the main following techniques based on (a) toposelective surface modification, (b) template-directed self-assembly, (c) controlled phase separation phenomena (d) controlled surface nucleation and e) microfluidic flow. Depending on the synthesis method used, several different morphologies of anisotropic particles could be generated such as snowman, acorn, dumbbells and half raspberry.

a. Toposelective surface modification

One of the most simple and intuitive methods to fabricate Janus particles involves the partial surface modification of one hemisphere of a spherical colloid, without altering the other. Different approaches have been applied to chemically modify the unprotected side of these monolayer surfaces (Figure 1.6). Surface modification of partially-masked particles (Figure 1.6a) involve particles been deposited into a removable material, such as a photoresist. Subsequently, thin non-continuous layers of metal or metal oxide were deposited using sputtering, before removing the photoresist layer. The anisotropic behaviour appeared after removal of the masking material of the particles. In the second method, the surface modification of one hemisphere of the particles is performed in reactive directional fluxes (Figure 1.6b). The second hemisphere will not be altered because it is protected by the particle itself so there is no need for masking steps. The particles need to be immobile during surface modification and are therefore arranged in a flat monolayer. The third method is derived from the microcontact printing technique (Figure 1.6c), which modifies only the surface of the contact area of the particles with the elastomeric stamp. After the preparation of the particle monolayer on a glass substrate, a surfactant film is deposited on a hydrophilic elastomeric stamp. Then the particle monolayer is stamped with the surfactant film and the polarized particles are re-dispersed in water. At high salt concentrations, the repulsion due to the net surface charge leads to the formation of primarily linear aggregates due to dipole interactions. The resulting Janus particles bare the stamped entities on one hemisphere establishing half-raspberry or snowman-like formations. The last method of surface modification of particles is through partial contact with reactive media (Figure 1.6d). In the first media the reacting molecules or particles are dissolved while the second is inert. As a result, the hemisphere facing the inert media remains intact while the other is modified.

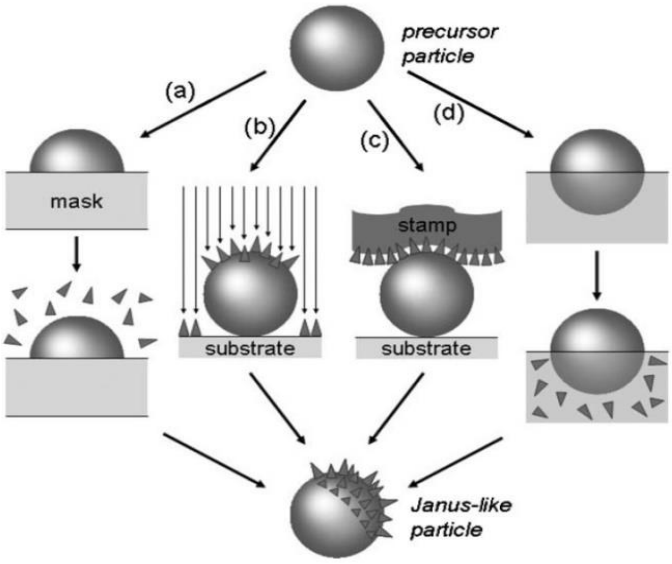

Figure 1.6: Schematic representation of the four strategies allowing to toposelectively modify the surface of particles. (a) masking/unmasking techniques, (b) techniques using reactive directional fluxes or fields, (c) microcontact printing techniques and (d) techniques based on interfaces and partial contact with a reactive medium.

b. Template directed self-assembly of particles

Template directed self-assembly of particles to produce Janus particles takes advantage of a patterned surface onto which a particle dispersion is allowed to dewet. Due to capillary forces the particles are trapped into a parallel cell, composed of two glass substrates (Figure 1.7) that confines spherical particles. The surface of the bottom substrate has been patterned with a array of cylindrical holes. When this dispersion was allowed to dewet slowly across the cell, the capillary force exerted on the rear edge of this liquid would drag the spherical particles across the surface of the bottom substrate until they were physically trapped in the hole arrays. The maximum number of particles that could be retained in each hole was determined by the ratio between the dimensions of the holes and the diameter of the particles.

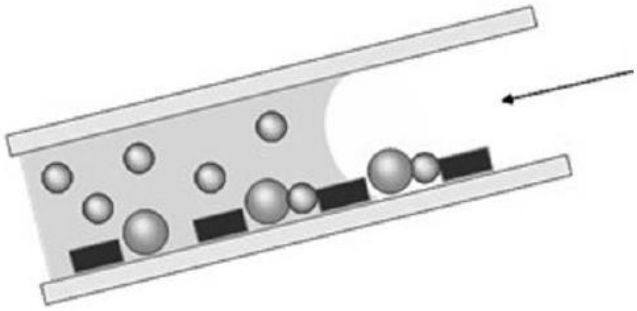

Figure 1.7: Schematic representation of the experimental cell and procedure for the dewetting on the second particle dispersion.

c. Controlled phase separation phenomena.

Controlled phase separation phenomena, such as the phase separation of polymer blends in emulsion droplets, is envisioned fairly facile and is especially useful for massive production of Janus particles. After evaporation of the solvent, phase separation leaves behind two incompatible polymer domains– Janus structures – in the resulting particles. The resulting snowman-like Janus particles are due to corruption of the silica and eruption of the silver core, which forms a silver iodine particle adjacent to the silica one. It also, allows the massive production of colloidal particles not only with Janus structural and chemical characteristics but also with Janus surface hydrophobicity.

d. Controlled surface nucleation.

The controlled surface nucleation technique to fabricate Janus particles is based on the controlled growth of a particle nucleated from the surface of a particle. This has been achieved using inorganic and metallic particles. The formations produced are usually 'snowman', 'acorn' and 'dumbbell'. The number and shape of the lobes nucleated of one particle can be controlled by varying the diameter and concentration of silica seeds and by varying the surface modification density. A major advantage of such synthetic pathways is the large-scale production of dissymmetric particles.

e. Microfluidics.

Microfluidic devices provide a powerful technique to manufacture Janus particles on the micrometric scale. Spherical chemically anisotropic Janus particles can be made through outflow of two monomers into a co-flow device before polymerization. Using a co-flow technique, many variations of Janus particles have been created. [9] , [24] , [25] Although generally confined to the micrometric scale, biphasic electrified outflow has also been used to obtain Janus droplets of nanoscale dimensions. Doyle *et al.* demonstrated by using a quadruple co-flow device, mask and UV source, that highly chemical and morphological anisotropic particles could be generated with very high precision.

1.4 Stimuli-responsive polymers

Synthetic polymers, which are designed to mimic the biopolymers, such as proteins, polysaccharides, and nucleic acids present as basic components in living organic systems, have been developed into a very active field due to their industrial and scientific value. They have been progressively developed to mimic the unique properties of biopolymers which are based on specific interactions, and exhibit abrupt physicochemical changes driven by small

environment changes. In the past decades, synthetic polymer systems that are responsive to external stimuli have been synthesized. Stimuli-responsive polymers are defined as polymers that change their physical or chemical properties such as their chain conformation, hydrophilicity, etc. in response to changes in the environmental conditions.

Physical stimuli such as temperature as well as chemical stimuli such as solution pH can alter the interactions between the polymer chains or between the polymer chains and the solvent. Responsive polymer systems are proposed for use in drug delivery, selective separation membranes and bioactive carriers. [26]

1.4.1 pH-responsive polymers

pH-responsive polymers consist of ionizable pendants groups that can accept or donate protons in response to changes of the pH. As the pH changes, the degree of ionization in a polymer bearing weakly ionizable groups is dramatically altered around a specific pH that is known as pK_a.

This rapid change in the net charge of the pendant groups causes an alternation of the hydrodynamic volume of the polymer chains. The transition from the collapsed state to the expanded state is explained by the osmotic pressure exerted by the mobile counterions neutralizing the polymer groups. Polymers that respond to pH changes normally consist of a hydrophobic backbone onto which ionizable weak acidic or basic groups are attached. Weak polyacids (Figure 1.8) accept protons at low pH and release protons at neutral and high pH. [27] On the other hand, polybases are neutral at high pH and become positively charged when protonated at neutral and low pH. [28]

Hydrophobically modified pH-responsive polymers have a sensitive balance between charged repulsion and hydrophobic interactions. When their ionizable pendants groups are protonated then hydrophobic properties dominate, which results to hydrophobic effects that causes aggregation of the polymer chains in an aqueous environment. Also another collapse mechanism of pH-responsive polymer systems is based on hydrogen bond formation between the hydrogen in the protonated group and an electron donating atom in other functional groups. This phenomenon occurs when the ionizable pendants groups are uncharged. [29]

1.4.1.1 Polyacids

Polyacids bear carboxylic acid side groups (Figure 1.8). In our case, poly(acrylic acid) (Figure 1.8 (a)) was used as a weak polyacid which exhibits an ionization/deionization transition from pH 4 to 8. Poly(acrylic acid) bearing carboxylic acid groups, is the most representative weak polyacid. Its carboxylic acid pendant groups accept protons at low pH,

while releasing them at high pH. Accordingly, at high pH values, electrostatic repulsion forces are present between the polymer chains. This gives a momentum to the hydrophobic interactions to govern the precipitation/solubilization of the polymer chains, the deswelling/swelling of hydrogels, or the hydrophobic/hydrophilic characteristics of polymer modified surfaces.

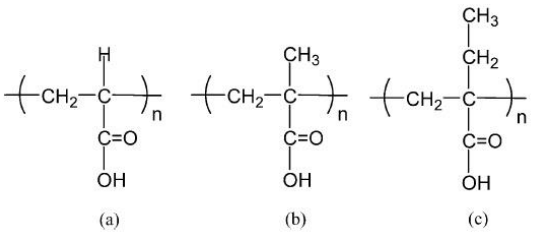

Figure 1.8: pH-responsive polyacids: (a) poly(acrylic acid) (PAA), (b) poly(methacrylic acid) (PMAA), (c) poly(2-ethyl acrylic acid) (PEAA).

1.4.1.2 Polybases

Polybases (Figure 1.9) have amine groups in their side chains which gain protons under acidic conditions and release them under basic conditions. One known polybase is PDEAEMA which has strong hydrophobic interactions at high pH values, also leading to "hypercoiled" conformations. PDEAEMA homopolymer undergoes an abrupt precipitation when the amino groups become deprotonated, due to hydrophobic interactions.

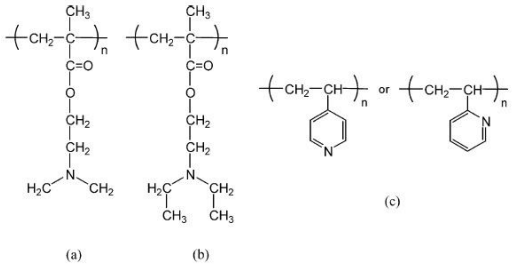

Figure 1.9: pH-responsive polybases: (a) Poly((N,N'-dimethylamino)ethyl methacrylate) (PDMAEMA), (b) poly((N,N-diethylamino)ethyl methacrylate) (PDEAEMA), (c) poly(4 or 2-vinylpyridine) (PVP).

1.5 Polymer-grafted particles

In nanotechnology, a particle is defined as a small object that behaves as a whole unit due to its transport and diffusion properties. Particles are further classified according to their diameter and shape. Nanoparticles are between 1 and 1000 nm in size and can have a wide variety of different shapes (rods, discs, spheres). A wide range of nanoparticles have been

reported (clay, silica, gold, C_{60}, carbon nanotubes). The surface coating of nanoparticles is crucial for determining their properties. Among the many inorganic/organic hybrid materials, silica-polymer hybrid materials are one of the most commonly reported in the literature. Surface functionalization of silica nanoparticles with polymer brushes is very important as the polymer coating alters the interfacial properties of the particles.

In general, the surface of inorganic materials is functionalized with polymer chains either chemically through covalent bonding or physically by physisorption (Figure 1.10). A disadvantage of physisorbed polymers is that they are unstable due to the relatively weak van der Waals forces or hydrogen bonding that anchors them to the surface. The grafting techniques such as "grafting to" or "grafting from" are preferred to maximize a stable interfacial compatibility between the two phases.

In the "grafting to" method, pre-formed, end-functionalized polymer chains are reacted with a chemically activated substrate to form a tethered polymer layer. This technique provides control of the polydispersity and the architecture of the polymer brushes at the surface, but the grafting densities are low because of steric crowding around the reactive sites by previously attached polymers. [30] In addition to that, the grafting reactions often require harsh conditions, e.g. high temperature and long reaction times which can induce the deterioration of the polymeric component.

Instead in the "grafting from" method a surface immobilized initiator is used to grow polymer chains in situ to generate a polymer brush. This technique results in significantly higher grafting densities. The active group is covalently attached onto the surface and therefore "grafting from" is non-reversible.

Using the right system and technique, one can control the functionality, density and thickness of the polymer brushes. Preparation of polymer brushes on silica can be accomplished by conventional free radical, controlled free radical, cationic, anionic and ring-opening metathesis polymerization techniques. [31]

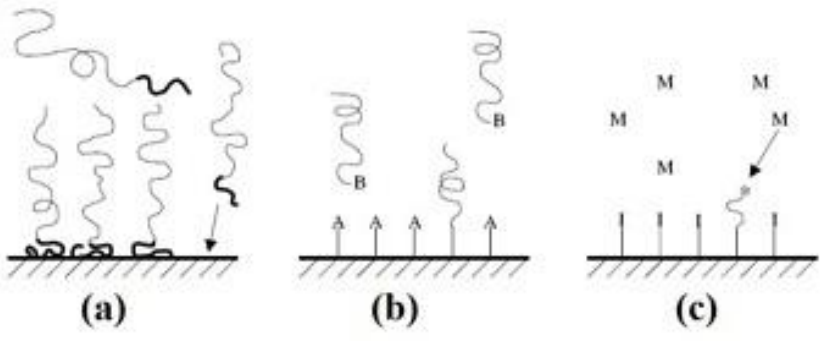

Figure 1.10: Schematic diagram of (a) physisorption, (b) "grafting to", (c) "grafting from".

1.6 Scope of this work

The present study focuses on the characterization of polyampholytic hybrid Janus nanoparticles comprising an inorganic silica core and a shell consisting of compartmentalized poly(*tert*-butyl acrylate) P(t-BuA) grafted polymer chains. The Janus particles comprise an amine-functionalized hemisphere and a grafted polymer on the other hemisphere. The hydrophobic polymer, P*t*-BuA, was grown using surface Atom Transfer Radial Polymerization (ATRP) from the one hemisphere of Janus initiator nanoparticles bearing contained ATRP initiating groups. The asymmetric decoration of the silica nanoparticles was revealed using scanning electron microscopy (SEM).

Acidic hydrolysis of P(t-BuA) resulted an oppositively charged polyampholitic Janus particles, with poly(acrylic acid) (PAA) chains on one hemisphere and an amine-functionalized hemisphere on the other side. The successful hydrolysis of P(t-BuA) was investigated by Fourier Transform Infrared (FT-IR) Spectroscopy and potentiometric titrations.

The amount of the grafting polymer chains from the surface was determined by Thermogravimetric Analysis (TGA) while the molecular weights and the molecular weight distributions of the polymers formed in solution were determined by Gel Permeation Chromatography (GPC). The pH-responsive behaviour of the particles with the hydrolysed polymer chains was investigated by potentiometric titrations and Dynamic Light Scattering (DLS).

CHAPTER 2. Experimental

2.1 Methods

2.1.1 Synthesis of hybrid Janus particles

The synthesis of the hybrid Janus nanoparticles with pH-responsive polymer chains is describes below. The Janus silica particles synthesized by Falireas Panagiotis. Polymer chains of hydrophobic poly(tert-butyl acrylate) P(t-BuA) were surface-initiated ATRP from the surface of ~100 nm silica nanoparticles. The synthetic route is depicted in Figure 2.1.

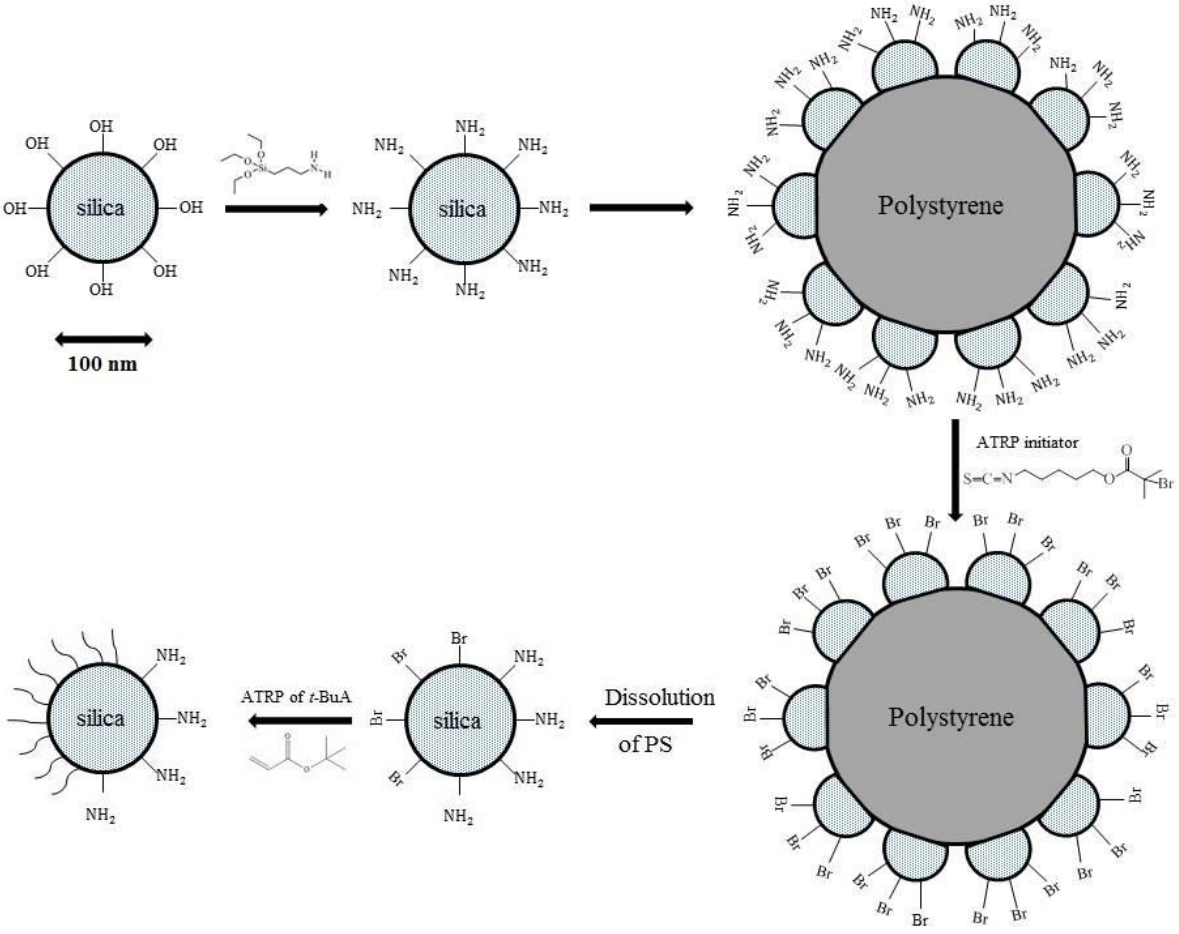

Figure 2.1: Schematic representation of the multistep reaction synthesis of Janus nanoparticles.

Initially, the modification of the SiO_2 particle surface with aminopropylsilane was carried out. Next, the synthesized amino-functionalized silica nanoparticles were used as stabilizers for the synthesis of a Pickering emulsion. The hybrid colloidosomes were prepared

using emulsion polymerization of styrene in the presence of the silica particles in methanol in order to form PS colloids stabilized by the silica particles.

Following the immobilization of the silica particles on the surface of the PS colloids, the ATRP initiator was reacted onto the exposed surface of the silica particles. The initiator was added in a dispersion of the $PS-SiO_2$ hybrid colloidosomes prepared above and the exposed amine groups on the surface of the silica particles were allowed to react with the isothiocyanate groups of the initiator. After the reaction, polystyrene was dissolved using toluene to yield after purification Janus nanoparticles bearing ATRP initiating sites.

Next, surface-initiated ATRP of t-BuA was carried out from the initiator-functionalized hemisphere of the silica nanoparticles followed by removal of the bromide end groups to obtain halogen free P(t-BuA) polymer chains. After synthesis amphiphilic hybrid Janus nanoparticles are obtained.

In the same solution mixture the free initiator Pentyl 2-bromo-2-methylpropanoate (PBMP) was added which led to the growth of free polymer chains. The free polymer formed during the polymerization is assumed to have the same molecular weight as that formed on the surface provided a fast exchange between the two polymer populations takes place.

2.1.2 Hydrolysis of P(*t*-BuA)

After synthesis the t-butyl groups of the P(t-BuA) polymer were hydrolysed (Figure 2.2) by acidic hydrolysis to yield SiO_2-PAA Janus nanoparticles. For this, in a 50 ml flask 1,4 dioxane was added followed by the addition of 0,1 gr of SiO_2-P(*t*-BuA) nanoparticles. The mixture was sonicated for 30 min and was left under continuous stirring for 1 hour. Then 1 ml of HCl (12 M) was added and the reaction mixture was degassed with dry nitrogen for 15 min. After 4 hours, the mixture was dried using a rotary evaporation and the nanoparticles were purified and dried for further use.

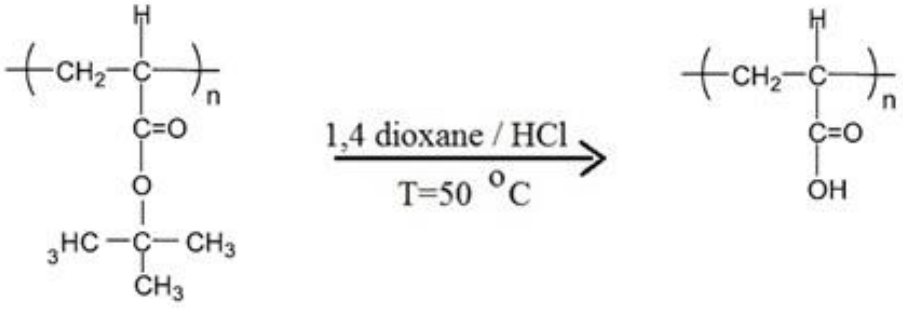

Figure 2.2: Hydrolysis reaction of P(*t*-BuA).

2.2 Experimental Techniques

2.2.1 Scanning Electron Microscopy (SEM)

Scanning Electron Microscopy (SEM) [32, 33] is a microscopy technique that uses electrons instead of light to form an image. Since their development in the early 1950's, scanning electron microscopes have developed new areas of study in the medical and physical science communities. SEM has allowed researchers to examine a much bigger variety of specimens. The scanning electron microscope has many advantages over traditional microscopes. The SEM has a large depth of field, which allows more of a specimen to be in focus at one time. The SEM also has much higher resolution, so closely spaced specimens can be magnified at much higher levels. Because the SEM uses electromagnets rather than lenses, the researcher has much more control in the degree of magnification. All of these advantages, as well as the actual strikingly clear images, make the scanning electron microscope one of the most useful instruments in research today.

A typical scanning electron microscope (SEM) (Figure 2.3) uses a focused beam of high-energy electrons to generate a variety of signals at the surface of solid specimens. The signals that are derived from electron-sample interactions reveal information about the sample including its external morphology (texture), chemical composition, and crystalline structure. In most applications, data are collected over a selected area of the surface of the sample, and a 2-dimensional image is generated that displays spatial variations in these properties. Areas ranging from approximately 1 cm to 5 microns in width can be imaged in a scanning mode using conventional SEM techniques (magnification ranging from 20X to approximately 30,000X, spatial resolution of 50 to 100 nm).

All samples must be of an appropriate size to fit in the specimen chamber and are generally mounted rigidly on a specimen holder called a specimen stub. For conventional imaging in the SEM, specimens must be electrically conductive, at least at the surface, and electrically grounded to prevent the accumulation of electrostatic charge at the surface. Conductive materials in current use for specimen coating include gold, gold/palladium alloy, platinum, and graphite. For a typical observation a solution of the sample in a good solvent is prepared and drop casted on a glass substrate. The dried sample is sputtered with gold to obtain a uniform 10 nm film and avoid charging. The measurements were carried out utilizing a scanning electron microscopy (FESEM; JEOL JSM 7000F) at an accelerating voltage of 10-30 kV.

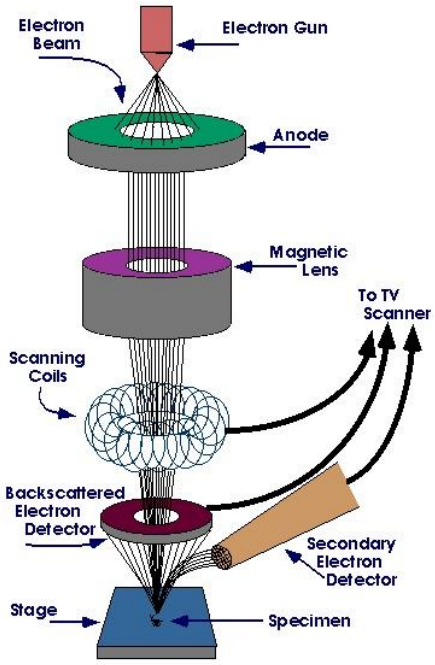

Figure 2.3: Schematic representation of a SEM.

2.2.2 Thermogravimetric Analysis (TGA)

Thermogravimetric analysis (TGA) is a method of thermal analysis in which changes in the mass of materials are measured as a function of increasing temperature (with constant heating rate), or as a function of time (with constant temperature). [34]. TGA can provide information about physical and chemical phenomena, physical, such as vaporization, sublimation, absorption, and chemical, such as desolvation (especially dehydration), and decomposition. TGA is commonly used to determine selected characteristics of materials that exhibit either mass loss or gain due to decomposition, oxidation, or loss of volatiles (such as moisture). Common applications of TGA are the material characterization through analysis of characteristic decomposition patterns, determination of organic and inorganic content in a sample, which may be useful for chemical analysis. It is an especially useful technique for the study of polymeric materials, including thermoplastics, thermosets, elastomers and composites.

Thermogravimetric analysis relies on a high degree of precision in three measurements: mass change, temperature, and temperature change at constant heating rate. Therefore, the basic instrumental requirements for TGA are a precision balance with the sample, and a programmable furnace which can be programmed for a constant heating rate. The TGA instrument continuously weighs a sample as it is heated to temperatures of up to 2000 ℃. As the temperature increases, various components of the sample are decomposed and the weight

percentage of each resulting mass change can be measured. Results are plotted with temperature on the X-axis and mass loss on the Y-axis. The data can be adjusted using curve smoothing and first derivatives are often also plotted to determine points of inflection for more in-depth interpretations.

The thermogravimetric analysis of the hybrid nanoparticles in this study was assessed with a Perkin Elmer Pyris Diamond TG/DTA (Figure 2.4) instrument under a nitrogen atmosphere. For a typical measurement ~10 mg of solid sample were placed in the furnace under a constant nitrogen flow ~150 bar and the temperature ramp was 10 ℃/min up to 800 ℃. The data was analyzed using the Diamond Pyris software.

Figure 2.4: Perkin Elmer Pyris Diamond TG/DTA.

2.2.3 Gel Permeation Chromatography (GPC)

Gel permeation chromatography (GPC) [35] is one of the most powerful and versatile analytical techniques available for understanding and predicting polymer performance. It is the most convenient technique for characterizing several important parameters. These include number average molecular weight, weight average molecular weight, Z weight average molecular weight, and the most fundamental characteristic of a polymer its molecular weight distribution. GPC separates the chains based on the size or hydrodynamic volume (radius of gyration) of the molecules. Separation occurs via the use of porous beads packed in a column (Figure 2.5). The smaller molecules can enter the pores more easily and therefore spend more time in these pores, increasing their retention time. Conversely, larger molecules spend little if any time in the pores and are eluted quickly. All columns have a range of molecular weights that can be separated. If a molecule is either too large or too small it will be either not retained or completely retained, respectively.

As can be inferred, there is a limited range of molecular weights that can be separated by each column and therefore the size of the pores for the packing should be chosen according to the range of molecular weight of analytes to be separated.

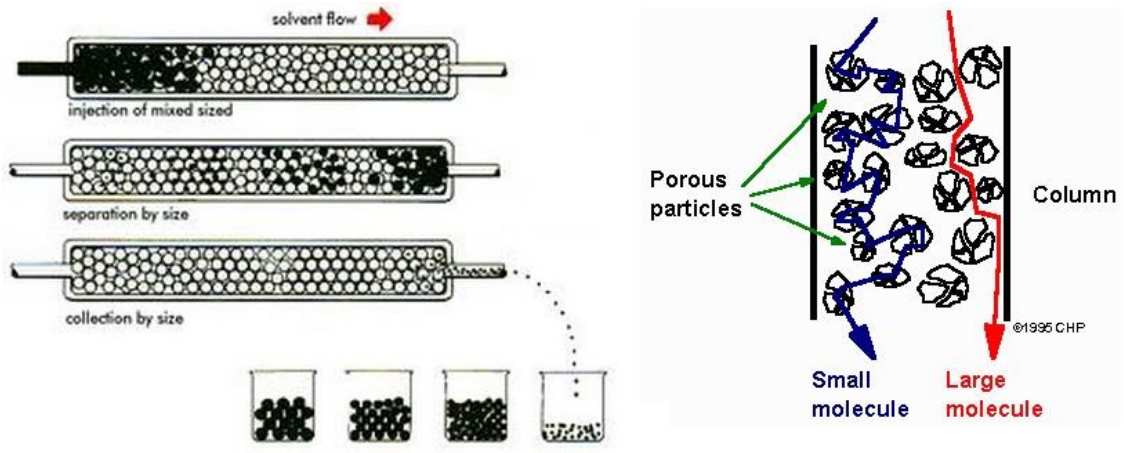

Figure 2.5: Schematic of a size-exclusion chromatography column.

In designing instrumentation for GPC, a variety of requirements must be satisfied. These are shown in the schematic representation of a basic gel permeation chromatograph (Figure 2.6) and are: injectors are needed to introduce the polymer solution into the flowing system, pumps deliver the sample and solvent through the columns and system, detectors monitor and record the separation, and data acquisition accessories control the test automatically, record the results, and calculate the molecular weight averages. The gel permeation chromatograph contains a number of different components that work together to provide optimum system performance with minimum effort.

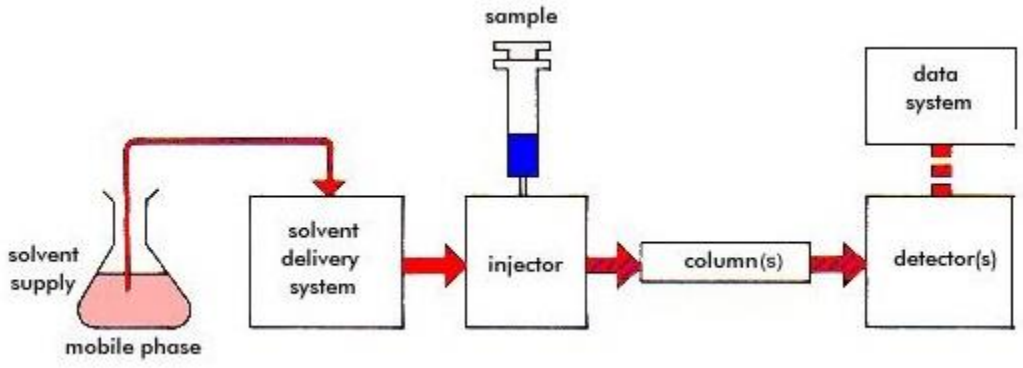

Figure 2.6: Schematic of a basic gel permeation chromatograph.

The molecular weights and the molecular weight distributions of the polymers formed in solution in this study were determined by gel permeation chromatography (GPC) utilizing a Thermo Finnigan chromatographer which included a TSP P1000 pump, two columns, Mixed-D and Mixed-E (Polymer Labs) and a refractive index (RI) detector (model ERC-RI 101). The software used for the analysis of the chromatograms was the Atlas Workstation and Cirrus GPC Reanalysis Software. The eluent used was a THF:TEA (50:1) mixture at a 1 mL/min flow rate. The calibration curve was based on eight narrow molecular weight linear PMMA standards ranging from 850 to 342,900 g/mol. In a typical measurement a 2 wt% solution of the sample was prepared in THF/TEA (50:1) and was injected to the system (20μL) at a column temperature set to 40℃ .

2.2.4 Fourier Transform Infared (FT-IR) Spectroscopy

Fourier Transform Infrared (FTIR) Spectroscopy [36] is a technique which is used to obtain an infrared spectrum of absorption, emission, photoconductivity of a solid, liquid or gas. An FTIR spectrometer simultaneously collects spectral data in a wide spectral range. This confers a significant advantage over a dispersive spectrometer which measures intensity over a narrow range of wavelengths at a time.

The goal of any absorption spectroscopy technique is to measure how a sample absorbs light at each wavelength. The most straightforward way to do this, the "dispersive spectroscopy" technique, is to shine a monochromatic light beam at a sample, measure how much of the light is absorbed, and repeat for each different wavelength. Nevertheless, Fourier transform spectroscopy is a less intuitive way to obtain the same information. Rather than shining a monochromatic beam of light at the sample, this technique shines a beam containing many frequencies of light at once, and measures how much of that beam is absorbed by the sample. Next, the beam is modified to contain a different combination of frequencies, giving a second data point. This process is repeated many times. Afterwards, a computer takes all these data and works backwards to infer what the absorption is at each wavelength.

In this study Fourier transform infrared (FT-IR) spectra were recorded on a Nicolet 6700 optical spectrometer equipped with a DTGS KBr detector. The spectra were collected in a range 400-4000 cm^{-1} at 128 scans and a resolution of 4 cm^{-1}.

2.2.5 Potentiometric Titrations

Titration is a common laboratory method of quantitative chemical analysis that is used to determine the unknown concentration of an identified acid or base. It makes use of the neutralization reaction that occurs between the acid and base. A titration curve (Figure 2.7) for an acid-base titration is a curve in the plane whose x axis is the volume of titrant added since the beginning of the titration and y axis is the pH of the solution. In an acid-base titration, the titration curve reflects the strength of the corresponding acid and base. The change in pH is small until the end point where there is a sharp change. The strength of an acid or base determines the sharpness of the change. For a strong acid and a strong base, the curve will be relatively smooth and very steep near the equivalence point. Because of this, a small change in titrant volume near the equivalence point results in a large pH change.

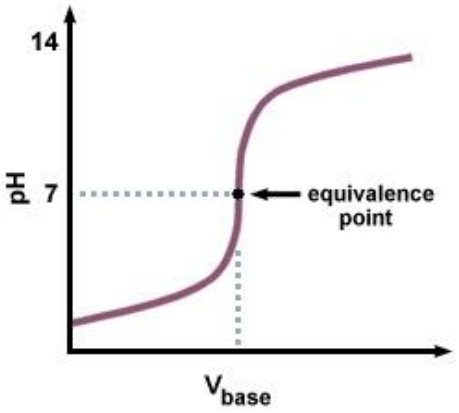

Figure 2.7: Titration curve of a strong base titrating a strong acid.

In the above curve, the beginning, the solution has a low pH and increases slowly as the strong base is added. As the solution approaches the point where all of the protons are neutralized, the pH rises sharply and then levels out again as the solution becomes more basic and more ions are added. The equivalent point occurs when the slope of the titration curve changes (see Figure 2.7) and can be calculated from the maximum of the first derivative of the data.

The titration of a weak acid with a strong base is different from that of a strong acid/base titration, primarily in the beginning of the titration, and with different equivalent point. There is a lag in reaching the equivalence point, as some of the weak acid is converted to its conjugate base. Moreover, the equivalent point itself is shifted upwards in pH. The reaction that occurs in the solution is:

$$HA\,(aq) + OH^-(aq) \rightleftharpoons A^-(aq) + H_2O\,(l)$$

As base is added, a buffer solution forms and the pH does not change rapidly until all of the weak acid reacts with the base. Analysis of the titration curve provides a mean for determining the dissociation constant of the acid. The pK_α of the acid is equal to the pH at the midpoint of the titration curve. This can be seen from the Henderson-Hasselbalch equation, which describes the weak acid equilibrium:

$$pH = pk_a + \log(\frac{[A^-]}{[HA]})$$

With $[A^-]$ the concentration of the basic form of the acid and [HA] the concentration of the acid. At the equivalent point $[A^-]$=[HA] and the second term of the right side of the Henderson-Hasselbalch equation becomes zero allowing to determine the pK_a from the pH.

Degree of ionization is defined as the ratio between the concentration of ionized units divided by the concentration of the total units in solution. It can be represented as a decimal number or as a percentage. In accordance, the fraction of charged carboxylic acid groups of the polymers used in this study is defined as the degree of ionization of the polymer. For PAA the degree of ionization is expressed as

$$\alpha = \frac{[PAA^-]}{[PAA] + [PAA^-]}$$

The effective pK_a value of the protonated monomer repeat units can be calculated from the Henderson-Hasselbalch equation at a degree of ionization α=0.5 where the concentration of protonated monomer repeat units is the same with the concentration of the unprotonated monomer repeat units.

In our study polyampholytic nanoparticles Janus-PAA (40 mgr) were dispersed in 40 gr of deionized water. The pH was adjusted to high pH values with the addition of few drops of NaOH 1M. The dispersion of the nanoparticles was titrated from pH 10 to 2 using HCl 0.01M under continuous stirring. The pH was monitored using a Thermo Russel (RL150) pH-meter.

2.2.6 Dynamic Light Scattering (DLS)

Light scattering is a very powerful method to characterize the structure of polymers and nanoparticles in solution [37]. Light scattering is a form of scattering in which light is the form of propagating energy which is scattered. Light scattering can be thought of as the deflection of a ray from a straight path, for example by irregularities in the propagation medium, particles, or at the interface between two media. Most objects that one sees are visible due to light scattering from their surfaces. Indeed, this is our primary mechanism of physical observation. Scattering of light depends on the wavelength or frequency of the light being

scattered. Since visible light has wavelength of the order of a micrometer, objects much smaller than this cannot be seen, even with the aid of a microscope. Colloidal particles as small as 1μm have been observed directly in aqueous suspension.

In a light-scattering experiment the quantity that is measured is the total scattered intensity I (q,t) at specific q (scattering wavevector),

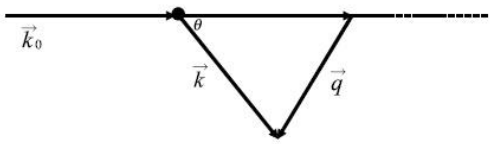

Figure 2.8: Sketch of the definition of the scattering vector $\vec{q} = \vec{k} - \overrightarrow{k_o}$.

where $\vec{k}$ and $\overrightarrow{k_o}$ are the wavevectors of the incident and of the scattered light beam and θ is the scattering angle. The scattering vector $\vec{q}$ is simply the difference of the two wavevectors and therefore,

$$|\vec{q}| = q = \frac{4\,\pi\, n_D \sin(\frac{\theta}{2})}{\lambda}$$

which can be used to extract information on the static and dynamic properties of the system, where n_D is the refractive index of the medium, λ the wavelength of the laser and θ the angle between the incident beam and the scattered beam.

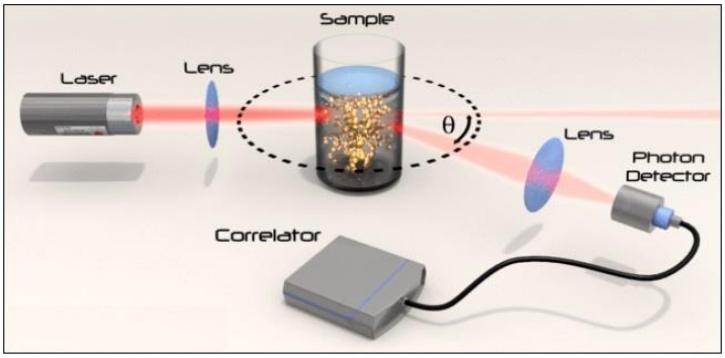

Figure 2.9: Schematic representation of light scattering.

Dynamic light scattering (DLS) (Figure 2.9) is one of the most popular light scattering techniques because it allows particle sizing down to 1 nm diameter. Typical applications are emulsions, micelles, polymers, proteins, nanoparticles or colloids. Dynamic light scattering is a technique that can be used to determine the size distribution profile of small particles in suspension or polymers in solution.

As mentioned above, if the scattering particles are moving, fluctuations in the scattered intensity with time are directly reflecting the so-called Brownian particle motion of the scattering particles. From a microscopic point of view the particles scatter the light and thereby imprint information about their motion. Analysis of the fluctuation of the scattered light thus yields information about the particles. Experimentally one characterizes intensity fluctuations by computing the intensity correlation function $g_2(t)$, whose analysis provides the diffusion coefficient of the particles.

$$g_2(q,t) = \frac{\langle I(q,t)I(q,t+\tau\rangle}{\langle I(q,t)^2\rangle}$$

where $g_2(q, \tau)$ is the autocorrelation function at a particular wave vector, q, and delay time, τ, and I is the intensity. The angular brackets $\langle \ \rangle$ denote the expected value operator, which in some texts is denoted by a capital E. At short time delays, the correlation is high because the particles do not have a chance to move to a great extent from the initial state that they were in. As the time delays become longer, the correlation decays exponentially, meaning that, after a long time period has elapsed, there is no correlation between the scattered intensity of the initial and final states. This exponential decay is related to the motion of the particles, specifically to the diffusion coefficient.

To obtain the diffusion coefficient the intensity correlation function must be analyzed. The standard procedure for this is by fitting a polynomial of third degree to the logarithm of the intensity correlation function. The decay rate Γ is calculated from the equation:

$$\Gamma = \frac{1}{\tau}$$

where τ is calculated from the Gaussian fit of the inverse Laplace. The decay rate is directly related to the diffusion coefficient D:

$$\Gamma = q^2 \cdot D_t \quad \text{, with } q = \frac{4\,\pi\, n_o}{\lambda}\,\sin\left(\frac{\theta}{2}\right) \ .$$

The Stokes-Einstein equation,

$$D_S = \frac{k_B T}{f} = \frac{k_B T}{6\pi\eta R_H} \Leftrightarrow R_H = \frac{k_B T}{6\pi\eta D_S}$$

allows one to determine the hydrodynamic radius R_H of the scattering particle, if sample temperature, T, and solvent viscosity, η, are known and the self-diffusion coefficient, D_S, is measured by dynamic light scattering . Note here that R_H is the radius of an equivalent sphere, experiencing during its Brownian motion in solution a friction f identical in magnitude to that of our scattering particle which itself is not necessarily a sphere.

The hydrodynamic radius R_H of the hybrid nanoparticles in the present study was measured using dynamic light scattering. The light source was an Oxxius solid state laser (SLIM 532) at a wavelength of 532 nm. The photo correlation was performed by an ALV-5000/E photon correlator. Scattering was collected at $30°, 40°, 50°, 60°, 90°, 120°, 150°$ scattering angles and the obtained time correlation functions were analyzed using KWW analysis. The concentration of the hybrid nanoparticles was all measurements was 0.005 w/w %.

CHAPTER 3. | Results and Discussion

3.1 Characterization of bare silica nanoparticles

3.1.1 Dynamic Light Scattering (DLS)

The pure silica nanoparticles were first characterized by DLS in order to determine their hydrodynamic size. DLS measurements were conducted at five different scattering angles. A single exponential decay of the intensity autocorrelation functions was observed, while the autocorrelation decay rate increased in a linear fashion over q^2, indicating uniform size particles and the absence of aggregates (Figure 3.1). The diffusion coefficient of the particles in THF calculated from the linear fit of the intensity autocorrelation decay rates was found to be $4{,}99 * 10^{-12}$ m^2/sec which according to Stokes-Einstein equation corresponds to a hydrodynamic radius of 89 nm. This measurement will be used as a reference for further results on the polymer-coated particles since THF was the solvent for all measurements.

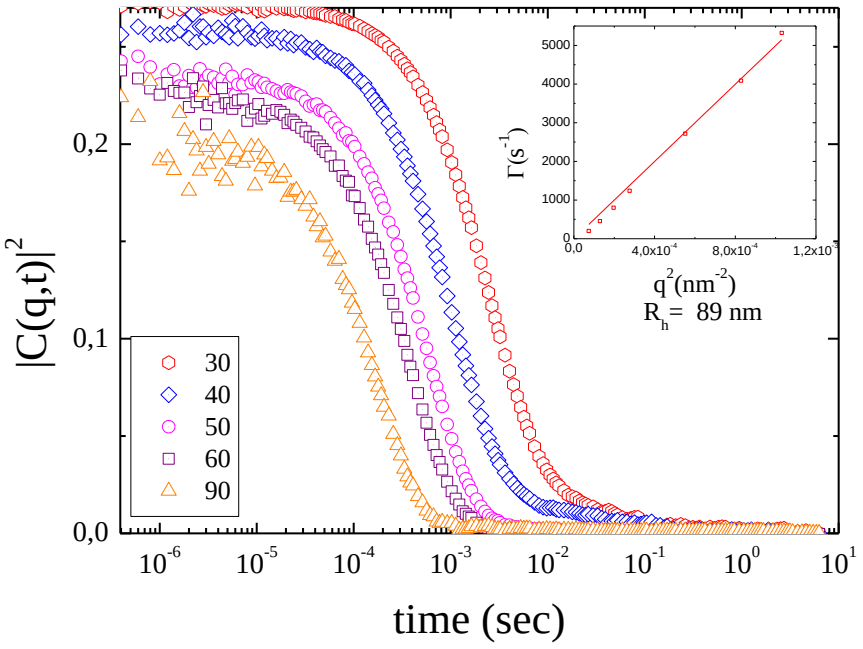

Figure 3.1: Intensity autocorrelation functions of the bare silica particles in THF at different scattering angles. Inset: Decay rates of the autocorrelation functions (Γ) as a function of the square wavevector (q^2).

3.1.2 Scanning Electron Microscopy (SEM)

Scanning Electron Microscopy (SEM) was used to obtain information concerning the size, shape, morphology and size distribution of the particles. The following figures shows scanning electron microscopy micrographs of bare silica nanoparticles from a THF solution c= 0.005 %. The bare silica particles were spherical in shape and monodisperse with a smooth, featureless surface morphology. These SEM images will be compared with SEM images of the Janus SiO_2-P(*t*-BuA) in order to identify the polymer coating. From the SEM images, the bare silica nanoparticles were found to have a size distribution in the range of 60-70 nm with average size 67 nm.

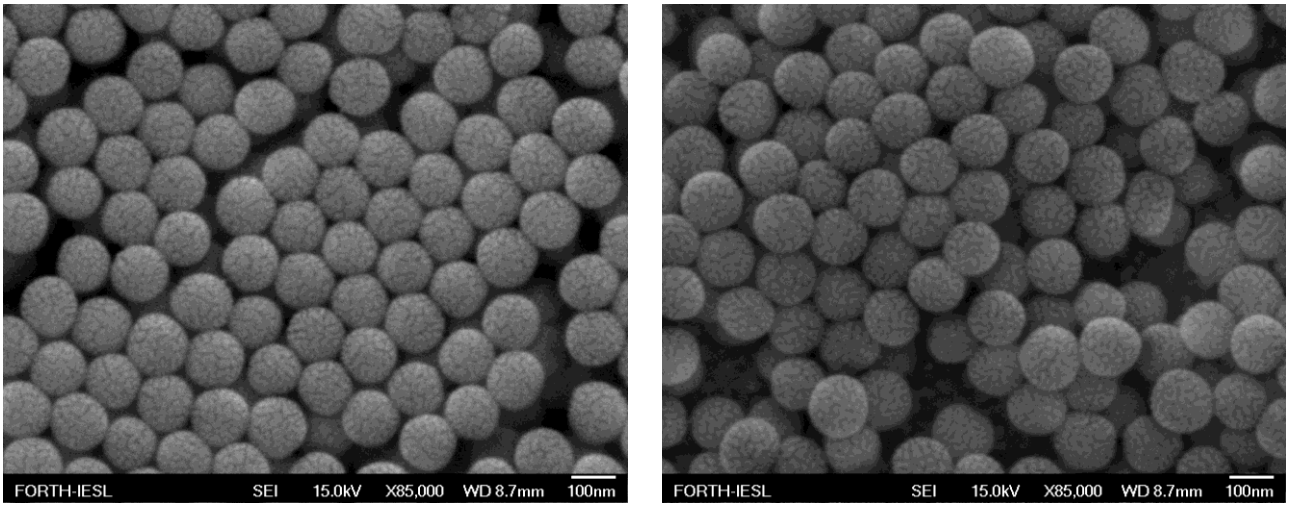

Figure 3.2: SEM images of bare silica particles.

3.2 Characterization of the hybrid Janus nanoparticles in organic solvents

3.2.1 Thermogravimetric Analysis (TGA)

In order to determine whether the hybrid Janus nanoparticles were successfully synthesized using the procedure described in the experimental section, TGA was performed. Typical TGA curves for the bare silica particles (green line), the Janus SiO_2-P(*t*-BuA) nanoparticles (black line) and P(*t*-BuA) homopolymer (red line) are depicted in Figure 3.3. The TGA curves show the % weight loss of the samples as a function of temperature. The % weight loss for the bare silica nanoparticles (green line) was found 8.85 %. This loss is mainly due to moisture which is physically absorbed on the surface of the particles possible contamination of the particle surface with organic matter and/or condensation of the surface silanol groups. In principle, the polymer loading can be determined from the difference in

weight loss between the bare silica nanoparticles and the Janus SiO_2-P(*t*-BuA) nanoparticles. A total 20.47 % weight loss was observed which was attributed to the decomposition of the organic content of the hybrids Janus nanoparticles. Moreover, Janus SiO_2-P(*t*-BuA) TGA curve exhibits a similar decomposition pattern to that for the P(t-BuA) homopolymer (red line).

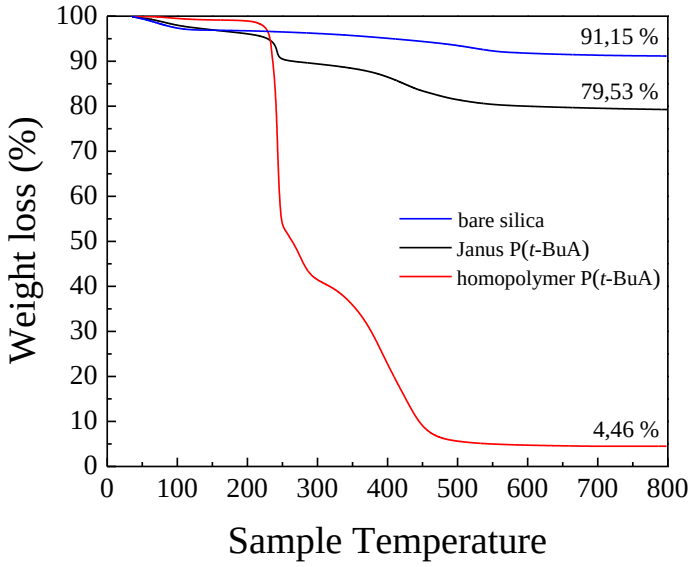

Figure 3.3: TGA thermograms of the bare silica nanoparticles, the Janus P(*t*-BuA) particles, and P(*t*-BuA) homopolymer.

3.2.2 Gel Permeation Chromatography (GPC)

The first step for the synthesis of the hybrid Janus nanoparticles was the ATRP initiation of t-BuA from Janus initiator nanoparticles in a solvent free polymerization in the presence of free initiator. The role of the free initiator was dual, first because of the small concentration of the surface initiator, it is necessary to generate enough copper II (deactivator of the reaction) to induce control of the polymerization. Second, the free polymer formed during the polymerization has been shown in the literature to have the same molecular weight with those formed on the particle surface. [38-40] This allows us to determine the molecular weight of the grafted polymer chains without etching the silica core using GPC.

Figure 3.4 shows the GPC chromatogram of the free P(t-BuA) polymer formed in solution in which a narrow peak is observed, indicative of a controlled polymerization. The molecular weight of the P(*t*-BuA) chains formed by the free initiator was found 265.800 g/mol and the polydispersity index is approximately 1.11. Thus, relatively monodisperse chains with an average molecular weight of 265.800 g/mol are grafted on the surface of the particles.

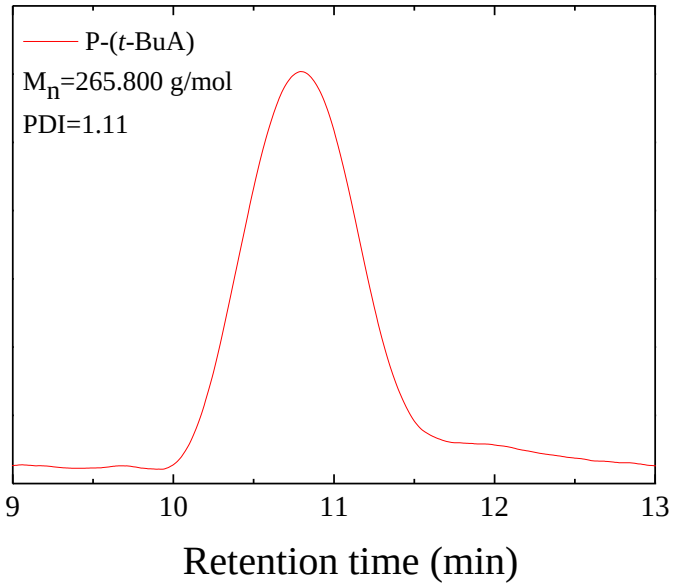

Figure 3.4: Chromatogram of the free polymer synthesized in solution during the synthesis of the Janus P(*t*-BuA) particles.

3.2.3 Scanning Electron Microscopy (SEM)

Scanning electron microscopy (SEM) was used to investigate the shape and size of the Janus SiO_2-P(*t*-BuA) particles. The sample preparation procedure for the SEM experiments involves first the dispersion of the Janus P(t-BuA) particles in a THF solution c=0,005 w/w %. Then a drop of this solution was placed on a silicon substrate, dried overnight at room temperature and next measured by SEM.

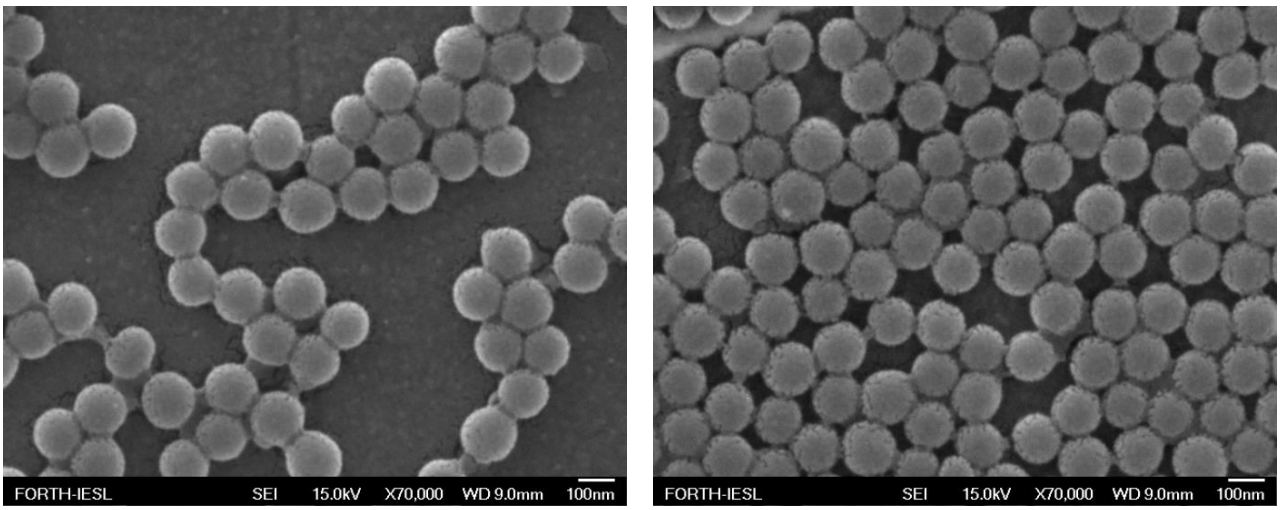

Figure 3.5: SEM images of the Janus P(t-BuA) from a dispersion in THF.

The SEM images above show particles which have a uniform size and a spherical shape. As we can see the particles are held together by a "sticky" material which is attributed to the polymer. However, no specific Janus morphology is observed in these SEM images. In order to demonstrate the anisotropic character of the hybrid nanoparticles, the particles were dispersed in a mixture of THF/water (1:9) solution. Afterwards a drop of this solution was placed on a silicon substrate and dried at room temperature. The SEM images following the above process are presented in Figure 3.6. Due to the hydrophobic interactions between the polymer chains in water the polymer is collapsed and phase separates from the silica particles. These SEM images reveal the characteristic dumbbell morphology of Janus particles.

The left image in Figure 3.6 shows a single Janus SiO_2-P(*t*-BuA) nanoparticle which consists of two parts. The part on the left is attributed to the silica sphere and is verified by the shape and size of the silica core. Whereas, the part on the right is attributed to the amorphous polymer grafted on the particle surface.

The image on the right in Figure 3.6 show doublets formed due to the hydrophobic attractions between the polymer modified surfaces in THF/water (1:9).

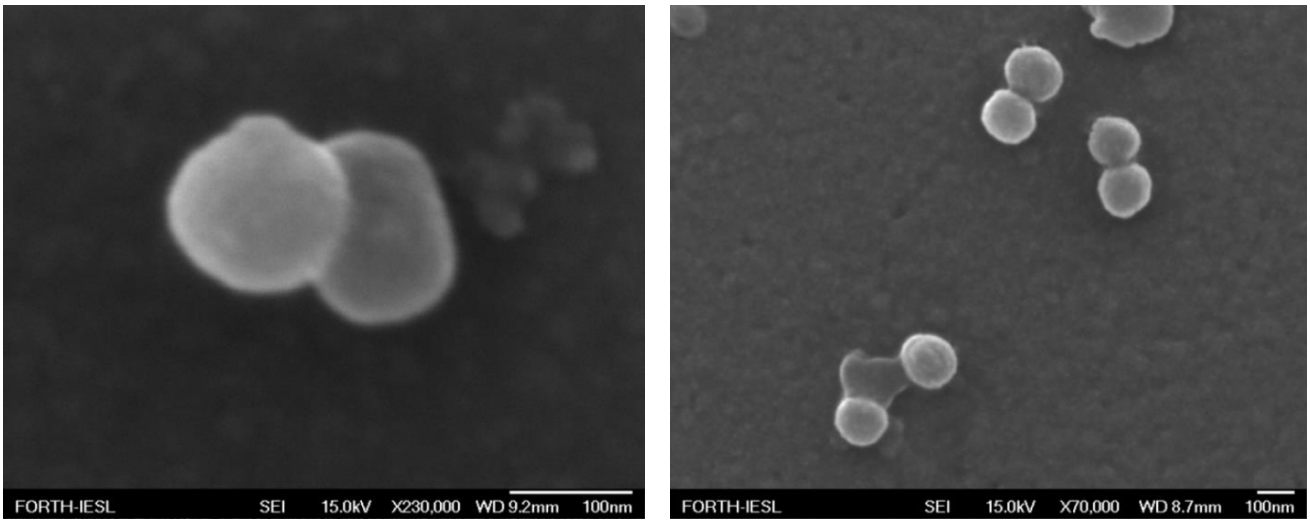

Figure 3.6: SEM images of the Janus P(*t*-BuA) from a dispersion in THF/water (1:9).

3.2.4 Dynamic Light Scattering (DLS)

The Janus SiO_2-P(*t*-BuA) particles were also characterized by DLS in order to determine their hydrodynamic radius. DLS measurements were conducted at five different scattering angles. Figure 3.7 shows a single exponential decay of the intensity autocorrelation functions, while the autocorrelation decay rate increased in a linear fashion as a function of q^2. This is indicated uniform size particles and the absence of aggregates. The diffusion coefficient of the Janus SiO_2-P(*t*-BuA) particles in THF calculated from the linear fit of the intensity autocorrelation decay rates was found to be $2.87 * 10^{-12}\ m^2$/sec which according to Stokes-Einstein equation corresponds to a hydrodynamic radius of 155 nm.

DLS measurement were carried out at Janus nanoparticles concentration c=0,005 w/w %. The hydrodynamic radius of the pure silica nanoparticles in THF was calculated 89 nm by DLS. For comparison, the corresponding hydrodynamic radius of the Janus SiO_2-P(*t*-BuA) nanoparticles in THF was found to increase to 155 nm by DLS, suggesting the successful grafting of P-*t*(BuA) on the surface of the silica nanoparticles.

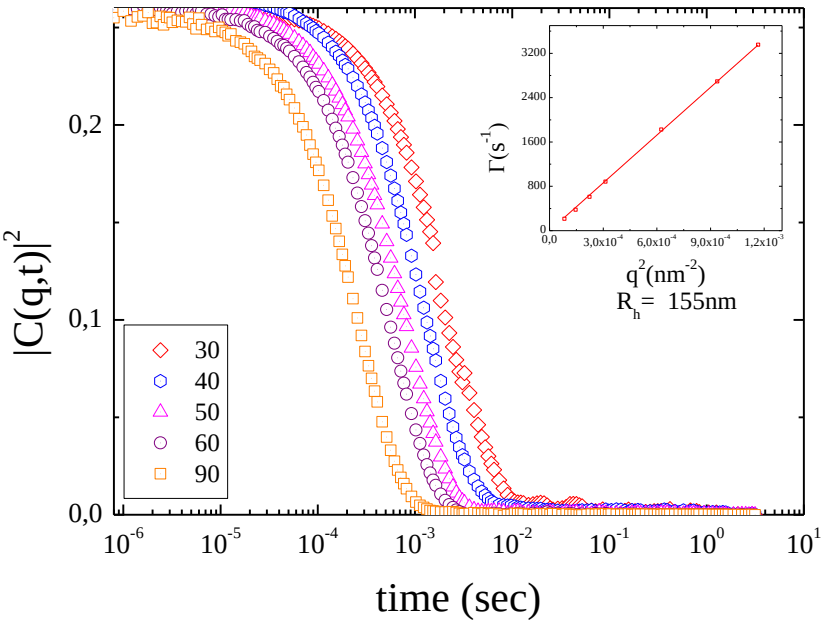

Figure 3.7: Intensity autocorrelation functions of the Janus P-t(BuA) nanoparticles in THF at different scattering angles. Inset: Decay rates of the autocorrelation functions (Γ) as a function of the square wavevector (q^2).

3.3 Characterization of the hybrid Janus nanoparticles in aqueous media

3.3.1 Hydrolysis of Janus SiO_2-P(*t*-BuA) nanoparticles

The Janus SiO_2-P(*t*-BuA) nanoparticles can be hydrolysed in acidic conditions to produce the anionic Janus SiO_2-PAA particles. The hydrolysis reaction is shown in Figure 3.8. Hydrolysis will give a polyampholytic character to the Janus SiO_2-PAA particles because the free hemisphere of the particles is functionalized with amine groups. Moreover, these particles present an interesting pH-responsive behaviour, as discussed below.

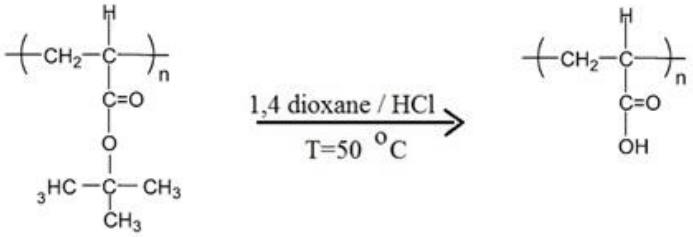

Figure 3.8: Hydrolysis of P(*t*-BuA) in acidic media.

The successful hydrolysis of the polymer was verified by FT-IR. Figure 3.9 shows FT-IR spectra for the Janus SiO_2-P(*t*-BuA) and the Janus SiO_2-PAA nanoparticles. The spectra was collected in the range 400-4000 cm^{-1} at 128 scans and a spectral resolution of 4 cm^{-1}.

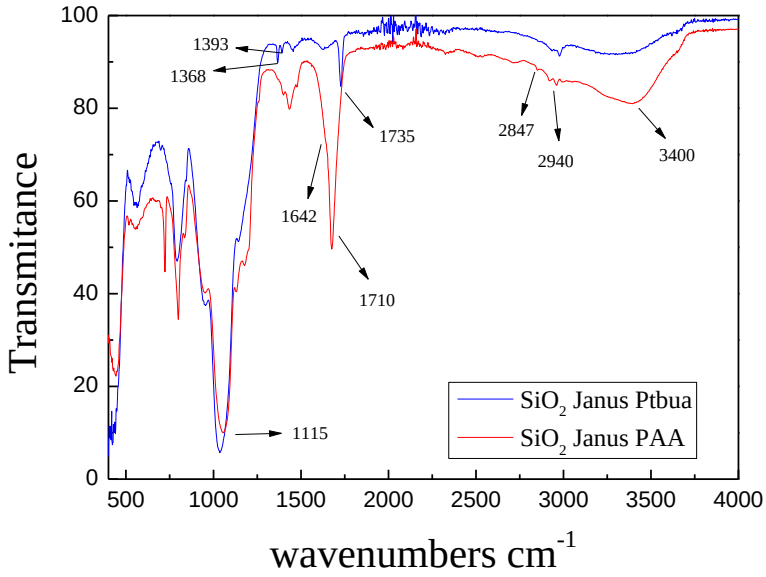

Figure 3.9: FT-IR spectra of the Janus SiO_2-P(*t*-BuA) and Janus SiO_2-PAA nanoparticles.

The *t*-butyl groups of P(*t*-BuA) were hydrolysed to form PAA residues. Previous studies have shown that the amine functionalized hemisphere is stable and intact under the acidic conditions used for the hydrolysis reaction.

As seen in Figure 3.9 both spectra exhibit an absorption band at 1115 cm^{-1} attributed to the Si-O-Si bond stretching of the silica particles. Moreover, for the Janus SiO_2-P(*t*-BuA) sample the absorption bands at 1368/1393 cm^{-1}, is due to the symmetric methyl deformation mode, whereas the absorption band at 1735 cm^{-1} corresponds to the strong C=O ester vibration. Finally, stretching vibration of the C-H bonds appears between 2847 cm^{-1} and 2940 cm^{-1} . On the other hand, in the FT-IR spectrum of the Janus SiO_2-PAA nanoparticles the doublet at 1368/1393 cm^{-1} disappears due to the loss of the asymmetric CH_3 stretching. Moreover, the carbonyl stretching vibration shifts slightly to 1710 cm^{-1} , corresponding to the acid carbonyl bond, and a shoulder at lower wavenumbers (1642 cm^{-1}) is observed, which is due to hydrogen bonded carbonyl groups. Finally, after hydrolysis the presence of a broad OH stretching vibration from 2900 to 3400 cm^{-1} is observed. These results verify the successful hydrolysis of the polymer ester bonds.

3.3.2 Aqueous solution properties of hybrid Janus SiO_2-PAA nanoparticles

The conformation of polyelectrolytes is very sensitive towards changes in ionic strength, pH and other external factors. It has to be emphasized that the ionic strength of the buffers used for these experiments was carefully kept constant at 0.1 M by addition of sodium chloride. The measurement of the Janus SiO_2-PAA nanoparticles in a solution of sodium chloride (NaCl) helps us to determine the size at ideal conditions due to the shielding effect on the carboxylic acid groups of PAA. The Na^+cations shield the carboxylate anions due to electrostatic interactions, and prevent the formation of aggregates.

The Janus SiO_2-PAA particles were first characterized by DLS in order to determine their hydrodynamic size in water and in the presence of NaCl. Figure 3.10 shows a single exponential decay of the intensity autocorrelation functions, while the autocorrelation decay rate increases in a linear fashion with q^2 . The diffusion coefficient of the Janus SiO_2-PAA nanoparticles in NaCl 0,1 M is calculated from the linear fit of the intensity autocorrelation decay rates and is found to be $1.73 * 10^{-12}\ m^2/sec$ which according to Stokes-Einstein equation corresponds to a hydrodynamic radius of 126 nm.

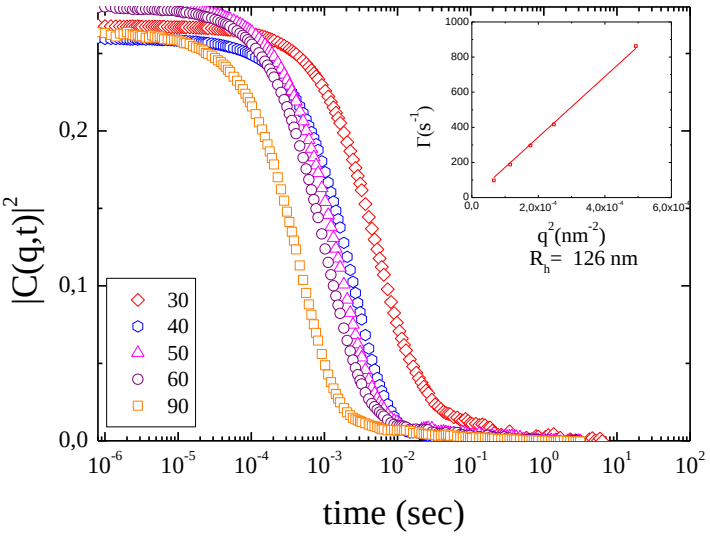

Figure 3.10: Intensity autocorrelation functions of the Janus SiO_2-PAA nanoparticles in 0,1 M NaCl at different scattering angles. Inset: Decay rates of the autocorrelation functions (Γ) as a function of the square wavevector (q^2).

The effect of solution pH on the Janus SiO_2-PAA nanoparticles behaviour was studied by potentiometric titration.[41] This process is fully reversible and can be retrieved upon addition of base or acid in the system. Titration curves were constructed in order to examine the response of the poly(acrylic acid) chains to pH changes and so to investigate their behaviour in aqueous solution.

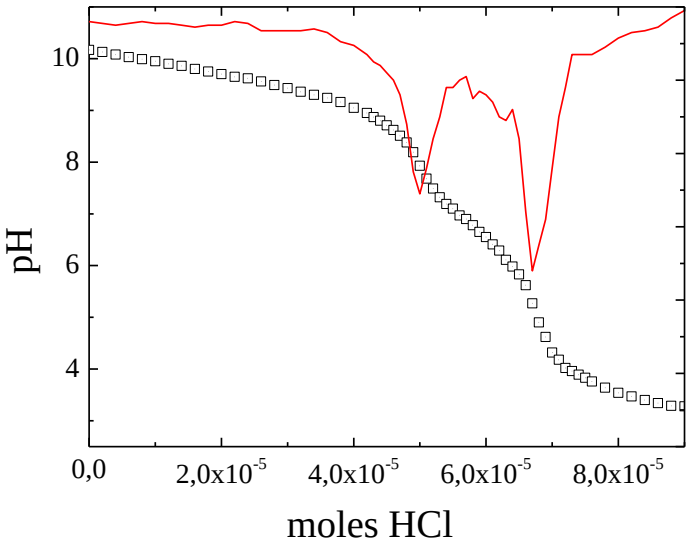

Figure 3.11: Titration curve for the Janus SiO_2-PAA nanoparticles at c=0,1 % w/w. (—) first derivative of the titration data.

Over all, the acid added at the beginning of the titration (pH > 9) neutralizes the excess base in the solution. However, at pH around 9, the addition of acid causes a rapid decrease of the pH to a value of ~ 8. At this point further addition of acid results in the protonation of the carboxylate groups of the polymer and the slight decrease of the pH (plateau region, see below). Finally, when the PAA units have become fully protonated an abrupt decrease of the solution pH is observed due to the excess acid added in the solution.

In the high pH regime (pH 8-9) the polymeric chains are fully ionized, while upon decreasing the solution pH the negative carboxylate groups of PAA become protonated. This reversible ionization process results in the appearance of a plateau in the titration curve of the PAA modified particles at a pH range between 5.5 and 8, as seen clearly in Figure 3.11.

As discussed in Chapter 2 the degree of ionization is defined as the ratio of the concentration of the ionized monomer repeat units divided by the concentration of the total monomer repeat units in the solution. For PAA the degree of ionization/protonation is expressed as:

$$\alpha = \frac{[\mathrm{PAA^-}]}{[\mathrm{PAA}] + [\mathrm{PAA^-}]}$$

Where $[\mathrm{PAA^-}]$ is the concentration of protonated PAA repeat units and [PAA] is the concentration of deprotonated PAA repeat units. The effective pK_a value of the protonated carboxylic acid groups is defined by Henderson-Hasselbalch equation:

$$\mathrm{pH} = \mathrm{pK}_a + \log\frac{[\mathrm{PAA^-}]}{[\mathrm{PAA}]}$$

At the midpoint of the plateau region the concentration of $[\mathrm{PAA^-}]$ is equal to the concentration of [PAA] and the second term of the Henderson-Hasselbalch equation becomes zero allowing the determination of the $\mathrm{pK_a}$ value. Practically, the $\mathrm{pK_a}$ value can be determined by a diagram of the solution pH versus the degree of protonation (α) at α=0,5.

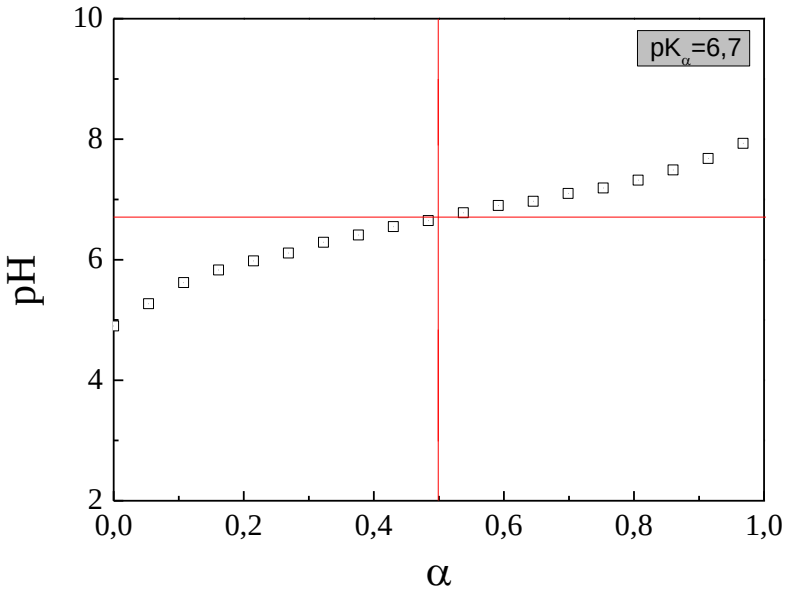

Figure 3.12: Solution pH versus degree of ionization for the Janus SiO_2-PAA nanoparticles.

Figure 3.12 shows the solution pH as a function of the degree of protonation in the range $0 < \alpha < 1$ for the Janus SiO_2-PAA nanoparticles. Values of α approximate the degree of protonation assuming that all of the H^+ from the added HCl protonate the carboxylic acid units. The small change of the pH as a function of α is attributed to the buffering capacity of the polymer at this pH region. The effective pK_α of the polymer was calculated quite accurately from this plot as the pH of the solution at a degree of ionization $\alpha = 0,5$ and was found 6,7.

In addition, the pK_α of free PAA as found in the literature is around 4.4 [42-44]. This difference is attributed to the crowding of the AA in the grafted polymer leading to a difficulty in the protonation of the PAA units near the surface of the particles. The concentration of the amino groups on the second hemisphere of the particles when compared to the carboxylic acid groups of PAA are negligible and for this reason they do not play significant role in the titration curve of the Janus SiO_2-PAA nanoparticles.

From the TGA results for the Janus SiO_2-P(*t*-BuA) nanoparticles the moles of *t*-BuA which are grafted on the silica particles were calculated and found to be $3,63 * 10^{-5}$. Moreover, from the titration data for the Janus SiO_2-PAA nanoparticles the moles of AA were calculated $1,68 * 10^{-5}$ which is in good agreement with the TGA results given the large error in the two techniques.

DLS measurements of an aqueous dispersion of the particles as a function of a well performed in order to assess the effect of the degree of ionization on the hydrodynamic size of the particles. These results are summarized in Table 3.1.

Table 3.1: Hydrodynamic radius of the Janus SiO_2-PAA nanoparticles for different degree of ionization.

R_h(nm)	a
104	0
117	0.27
136	0.65
166	0.97

The hydrodynamic radius at a degree of ionization equal to α=0.97 when all the carboxylic acid groups are deprotonated was found to be 166 nm. This value is considerably higher than the one found for the Janus SiO_2-P(*t*-BuA) particles in THF, and is attributed to the electrostatic repulsions among the charged polymer chains that drive the polymer to adapt an extended conformation in solution. At a lower degree of ionization α=0.65 the hydrodynamic radius was found to decrease and equals to 136 nm. At an even lower degree of ionization α =0.27, the hydrodynamic radius decreases further to 117 nm. Upon further deprotonation of the particles, the hydrodynamic radius decreases further to 104 nm.

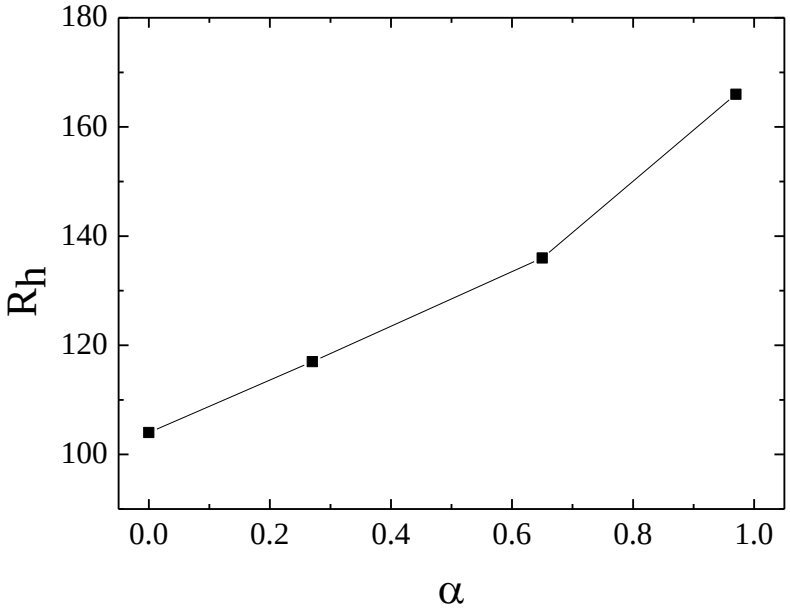

Figure 3.14: Hydrodynamic radius of the Janus SiO_2-PAA particles as a function of the degree of ionization.

As seen in Figure 3.14, when increasing the solution pH and therefore degree of ionization of the polymer there is a concomitant increase in nanoparticle size. PAA bearing the carboxylic acid groups accepts protons at low pH, and releases them at high pH. The increase in nanoparticle size with degree of ionization is due to the ionization of the grafted PAA chains on the silica surface. As, the acid groups along the polymer backbone become deprotonated, Coulombic repulsions between of the same charges force the polymer to adopt an extended conformation, which results in an increase in the nanoparticle size.[45] At the point where the polymer chains becomes fully ionized all of the counterions should remain trapped within the PAA layer, and the overall size of the nanoparticle will be determined by the balance between osmotic pressure created the counterions and polymer chain elasticity. [46, 47] It is also interesting to observe that at very high pH values the nanoparticle collapses because the addition of further ions through continued increasing pH will have a similar effect to adding salt. Since the fully ionized PAA retains its counterions within the polymer layer to retain electron neutrality.

CHAPTER 4. Conclusions

The scope of this work was to characterize polymer-silica Janus nanoparticles. These particles comprise one polymer grafted hemisphere and a free hemisphere and were synthesized using surface-initiated ATRP. The free hemisphere was covered by amino groups from the APTES which was used to modify the particle surface. The selection of the hydrophobic poly(*tert*-butyl acrylate) was because the methacrylate ester can be hydrolysed to form pH-responsive poly(acrylic acid) particles which are hydrophilic.

The successful synthesis of the Janus polymer-silica particles was verified by TGA, while the controlled nature of the polymerization reaction was confirmed with GPC. The size of the particles was evaluated by DLS measurements, while SEM images provided insight on the topology of the Janus particles.

Subsequent hydrolysis of the *tert*-butyl ester groups of the P(*t*-BuA) grafted chains resulted in the formation of hybrid Janus nanoparticles which exhibited pH responsive behaviour in aqueous solution due to the presence of both ionizable hemispheres. The successful hydrolysis was proved by FT-IR spectroscopy.

Potentiometric titrations of the Janus SiO_2-PAA in aqueous solution exhibited a simultaneous ionization process due to the similar buffer zones of the acidic and basic units of the AA and amino groups of APTES respectively present on the surface of the particles. Also, from the potentiometric titration of the Janus SiO_2-PAA particles the pK_α was calculated. The pH-depended size of the Janus PAA particles was shown by DLS measurements verifying the pH-responsive behaviour of the Janus particles.

DLS measurements show that when the pH increases the particle size also increases, due to electrostatic repulsion between the protonated carboxylic acid groups of PAA.

These silica PAA Janus nanoparticles present an excellent response to solution pH and are attractive among others for controlled uptake and release applications.

References

1. Perro, A., et al., *Design and synthesis of Janus micro- and nanoparticles.* Journal of Materials Chemistry, 2005. **15**(35-36): p. 3745-3760.
2. Loget, G. and A. Kuhn, *Bulk synthesis of Janus objects and asymmetric patchy particles.* Journal of Materials Chemistry, 2012. **22**(31): p. 15457-15474.
3. Du, J. and R.K. O'Reilly, *Anisotropic particles with patchy, multicompartment and Janus architectures: preparation and application.* Chem Soc Rev, 2011. **40**(5): p. 2402-16.
4. Li, F., D.P. Josephson, and A. Stein, *Colloidal Assembly: The Road from Particles to Colloidal Molecules and Crystals.* Angewandte Chemie International Edition, 2011. **50**(2): p. 360-388.
5. Lattuada, M. and T.A. Hatton, *Synthesis, properties and applications of Janus nanoparticles.* Nano Today, 2011. **6**(3): p. 286-308.
6. Granick, S., S. Jiang, and Q. Chen, *Janus particles.* Print edition, 2009. **62**(7): p. 68-69.
7. Walther, A. and A.H.E. Muller, *Janus particles.* Soft Matter, 2008. **4**(4): p. 663-668.
8. *Janus particle synthesis, self-assembly and applications*. RSC smart materials2012, Cambridge, UK :: RSC Pub. xx, 292 p. : ill. (some col.) ; 25 cm.
9. Nie, Z., et al., *Janus and Ternary Particles Generated by Microfluidic Synthesis: Design, Synthesis, and Self-Assembly.* Journal of the American Chemical Society, 2006. **128**(29): p. 9408-9412.
10. Erhardt, R., et al., *Janus Micelles†.* Macromolecules, 2001. **34**(4): p. 1069-1075.
11. Walther, A., et al., *Janus Discs.* Journal of the American Chemical Society, 2007. **129**(19): p. 6187-6198.
12. Dendukuri, D., T.A. Hatton, and P.S. Doyle, *Synthesis and Self-Assembly of Amphiphilic Polymeric Microparticles.* Langmuir, 2006. **23**(8): p. 4669-4674.
13. Hong, L., et al., *Clusters of Charged Janus Spheres.* Nano Letters, 2006. **6**(11): p. 2510-2514.
14. Hong, L., et al., *Clusters of Amphiphilic Colloidal Spheres.* Langmuir, 2008. **24**(3): p. 621-625.
15. Goyal, A., C.K. Hall, and O.D. Velev, *Phase diagram for stimulus-responsive materials containing dipolar colloidal particles.* Physical Review E, 2008. **77**(3): p. 031401.
16. Q, C., et al., - *Supracolloidal reaction kinetics of Janus spheres.* Science, 2011. **331**(6014): p. 199-202.

17. Binks, B.P. and P.D.I. Fletcher, *Particles Adsorbed at the Oil−Water Interface: A Theoretical Comparison between Spheres of Uniform Wettability and "Janus" Particles.* Langmuir, 2001. **17**(16): p. 4708-4710.
18. Nisisako, T., et al., *Synthesis of Monodisperse Bicolored Janus Particles with Electrical Anisotropy Using a Microfluidic Co-Flow System.* Advanced Materials, 2006. **18**(9): p. 1152-1156.
19. Behrend, C.J., J.N. Anker, and R. Kopelman, *Brownian modulated optical nanoprobes.* Applied Physics Letters, 2004. **84**(1): p. 154-156.
20. Behrend, C.J., et al., *Metal-Capped Brownian and Magnetically Modulated Optical Nanoprobes (MOONs): Micromechanics in Chemical and Biological Microenvironments†.* The Journal of Physical Chemistry B, 2004. **108**(29): p. 10408-10414.
21. Anker, J.N., et al., *Magnetically-modulated optical nanoprobes (MagMOONs) and systems.* Journal of Magnetism and Magnetic Materials, 2005. **293**(1): p. 655-662.
22. Howse, J.R., et al., *Self-Motile Colloidal Particles: From Directed Propulsion to Random Walk.* Physical Review Letters, 2007. **99**(4): p. 048102.
23. Golestanian, R., T.B. Liverpool, and A. Ajdari, *Propulsion of a Molecular Machine by Asymmetric Distribution of Reaction Products.* Physical Review Letters, 2005. **94**(22): p. 220801.
24. Kim, S.-H., et al., *Magnetoresponsive Microparticles with Nanoscopic Surface Structures for Remote-Controlled Locomotion.* Angewandte Chemie International Edition, 2010. **49**(22): p. 3786-3790.
25. Chen, C.-H., et al., *Janus Particles Templated from Double Emulsion Droplets Generated Using Microfluidics.* Langmuir, 2009. **25**(8): p. 4320-4323.
26. Yang, C.-C., et al., *New environmentally responsive fluorescent N-isopropylacrylamide copolymer and its application to DNA sensing.* Journal of Polymer Science Part A: Polymer Chemistry, 2006. **44**(19): p. 5495-5504.
27. Philippova, O.E., et al., *pH-Responsive Gels of Hydrophobically Modified Poly(acrylic acid).* Macromolecules, 1997. **30**(26): p. 8278-8285.
28. Pinkrah, V.T., et al., *Physicochemical Properties of Poly(N-isopropylacrylamide-co-4-vinylpyridine) Cationic Polyelectrolyte Colloidal Microgels.* Langmuir, 2003. **19**(3): p. 585-590.
29. Aoki, T., et al., *Temperature-Responsive Interpenetrating Polymer Networks Constructed with Poly(acrylic acid) and Poly(N,N-dimethylacrylamide).* Macromolecules, 1994. **27**(4): p. 947-952.
30. Lyatskaya, Y. and A.C. Balazs, *Modeling the Phase Behavior of Polymer−Clay Composites.* Macromolecules, 1998. **31**(19): p. 6676-6680.
31. Radhakrishnan, B., R. Ranjan, and W.J. Brittain, *Surface initiated polymerizations from silica nanoparticles.* Soft Matter, 2006. **2**(5): p. 386-396.

32. Egerton, R., *An Introduction to Microscopy*, in *Physical Principles of Electron Microscopy*2005, Springer US. p. 1-25.
33. Reimer, L., *Scanning Electron Microscopy: Physics of Image Formation and Microanalysis, Second Edition.* Measurement Science and Technology, 2000. **11**(12): p. 1826.
34. Coats, A.W. and J.P. Redfern, *Thermogravimetric analysis. A review.* Analyst, 1963. **88**(1053): p. 906-924.
35. Ouano, A.C., *Gel-permeation chromatography. VII. Molecular weight detection of GPC effluents.* Journal of Polymer Science Part A-1: Polymer Chemistry, 1972. **10**(7): p. 2169-2180.
36. Gerwert, K. and C. Kötting, *Fourier Transform Infrared (FTIR) Spectroscopy*, in *eLS*2001, John Wiley & Sons, Ltd.
37. *Fundamental Concepts*, in *Light Scattering from Polymer Solutions and Nanoparticle Dispersions*2007, Springer Berlin Heidelberg. p. 1-24.
38. Kizhakkedathu, J.N., R. Norris-Jones, and D.E. Brooks, *Synthesis of Well-Defined Environmentally Responsive Polymer Brushes by Aqueous ATRP.* Macromolecules, 2004. **37**(3): p. 734-743.
39. Liu, T., et al., *Water-Dispersible Carbon Black Nanocomposites Prepared by Surface-Initiated Atom Transfer Radical Polymerization in Protic Media.* Macromolecules, 2005. **39**(2): p. 548-556.
40. Ejaz, M., et al., *Controlled Graft Polymerization of Methyl Methacrylate on Silicon Substrate by the Combined Use of the Langmuir−Blodgett and Atom Transfer Radical Polymerization Techniques.* Macromolecules, 1998. **31**(17): p. 5934-5936.
41. Boyes, S.G., et al., *Synthesis, Characterization, and Properties of Polyelectrolyte Block Copolymer Brushes Prepared by Atom Transfer Radical Polymerization and Their Use in the Synthesis of Metal Nanoparticles.* Macromolecules, 2003. **36**(25): p. 9539-9548.
42. Gebhardt, J.E. and D.W. Fuerstenau, *Adsorption of polyacrylic acid at oxide/water interfaces.* Colloids and Surfaces, 1983. **7**(3): p. 221-231.
43. Kurkuri, M.D. and T.M. Aminabhavi, *Poly(vinyl alcohol) and poly(acrylic acid) sequential interpenetrating network pH-sensitive microspheres for the delivery of diclofenac sodium to the intestine.* Journal of Controlled Release, 2004. **96**(1): p. 9-20.
44. Mahaveer, D.K., et al., *Electroactive behavior of poly(acrylic acid) grafted poly(vinyl alcohol) samples, their synthesis using a Ce (IV) glucose redox system and their characterization.* Smart Materials and Structures, 2006. **15**(2): p. 417.
45. Mori, H., et al., *Hybrid Nanoparticles with Hyperbranched Polymer Shells via Self-Condensing Atom Transfer Radical Polymerization from Silica Surfaces.* Langmuir, 2002. **18**(9): p. 3682-3693.
46. Laguecir, A., et al., *Size and pH effect on electrical and conformational behavior of poly(acrylic acid): Simulation and experiment.* European Polymer Journal, 2006. **42**(5): p. 1135-1144.

47. Lizhong, J., et al., *Synthesis and characterization of stimuli-responsive poly(acrylic acid) grafted silica nanoparticles.* Smart Materials and Structures, 2007. **16**(6): p. 2169.